JOURNAL OF GEOPHYSICAL RESEARCH, VOL. 113, B09210, doi:10.1029/2007JB005540, 2008

Water contents in mantle xenoliths from the Colorado Plateau and vicinity: Implications for the mantle rheology and hydration-induced thinning of continental lithosphere

Zheng-Xue Anser Li,[1] Cin-Ty A. Lee,[1] Anne H. Peslier,[2,3] Adrian Lenardic,[1] and Stephen J. Mackwell[4]

Received 4 December 2007; revised 5 May 2008; accepted 24 June 2008; published 26 September 2008.

[1] Nominally anhydrous minerals (e.g., olivine, clinopyroxene, and orthopyroxene) in peridotite xenoliths collected from the Colorado Plateau and southern Basin and Range in western North America were systematically analyzed by Fourier transform infrared spectroscopy for water contents. Measured water contents range from 2 to 45 ppm for olivine, from 53 to 402 ppm for orthopyroxene, and from 171 to 957 ppm for clinopyroxene. The Colorado Plateau has the highest water contents (up to 45 ppm H_2O in olivine, 402 ppm H_2O in orthopyroxene, and 957 ppm H_2O in clinopyroxene), while San Carlos in the southern Basin and Range has the lowest water contents (up to 4 ppm H_2O in olivine, 82 ppm H_2O in orthopyroxene, and 178 ppm H_2O in clinopyroxene). With the exception of San Carlos, the olivine and pyroxenes from all other localities (Dish Hill, Grand Canyon, and Navajo) have water contents close to or higher than that inferred for the fertile asthenospheric mantle. We interpret the high water contents measured here to have been introduced into the base of the lithospheric mantle by rehydration associated with the subduction of the Farallon plate beneath North America during the early Cenozoic. Application of an updated flow law for dislocation creep of wet olivine to lithospheric mantle conditions beneath the Colorado Plateau predicts that for a given background shear stress, hydration alone can result in approximately 1 order of magnitude drop in the effective viscosity at the base of the lithosphere. If viscosity alone is used to distinguish the lithosphere from underlying asthenosphere, this suggests that hydration could have resulted in more than 10 km of lithospheric thinning. Viscosity reduction and lithospheric thinning of even larger extents (up to ~100 km) are predicted when thicker lithosphere (such as Archean cratons) and larger water contents (up to water-saturated conditions) are considered. If our interpretations are correct, the implications of our study go beyond western North America and hint at a possible way of recycling continental mantle, including cratonic mantle, back into the convecting mantle.

Citation: Li, Z.-X. A., C.-T. A. Lee, A. H. Peslier, A. Lenardic, and S. J. Mackwell (2008), Water contents in mantle xenoliths from the Colorado Plateau and vicinity: Implications for the mantle rheology and hydration-induced thinning of continental lithosphere, *J. Geophys. Res.*, *113*, B09210, doi:10.1029/2007JB005540.

1. Introduction

[2] Cratons are the ancient (Precambrian) cores of continents that have, for the most part, remained tectonically quiescent over billion year timescales. The lithospheric mantle roots beneath cratons are found to be thicker and more refractory, that is melt-depleted, than most Phanerozoic lithospheres [e.g., *Hawkesworth and Norry*, 1983; *Jordan*, 1978; *Menzies and Hawkesworth*, 1987; *Nixon*, 1987]. These depleted mantle roots, together with the overlying crust, are thought to be chemically buoyant and strong enough to resist convective disruption on billion year timescales [*Doin et al.*, 1997; *Griffin et al.*, 1999, 2003; *Jordan*, 1975, 1978; *Lee et al.*, 2005; *Lee*, 2006; *Lenardic and Moresi*, 1999; *Lenardic et al.*, 2003; *Pearson et al.*, 1995; *Pollack*, 1986; *Sengor*, 1999; *Shapiro et al.*, 1999]. Part of this lithospheric strength is attributed to the cooler thermal state of cratons [*Jordan*, 1978; *Pollack*, 1986], but cool temperatures alone are insufficient to prevent disruption by mantle convection over prolonged geological time as thermal reequilibration should also occur within billion year timescales. Cratonic mantle roots may also be intrinsically strong because they were dehydrated during melt depletion, resulting in a dry residue compared to the "damp" fertile mantle making up most of the mantle [*Hirth and Kohlstedt*,

[1]Department of Earth Sciences, Rice University, Houston, Texas, USA.
[2]Jacobs Technology, ESCG, Houston, Texas, USA.
[3]Astromaterials Research and Exploration Science, NASA Johnson Space Center, Houston, Texas, USA.
[4]Lunar and Planetary Institute, Houston, Texas, USA.

0148-0227/08/2007JB005540$09.00

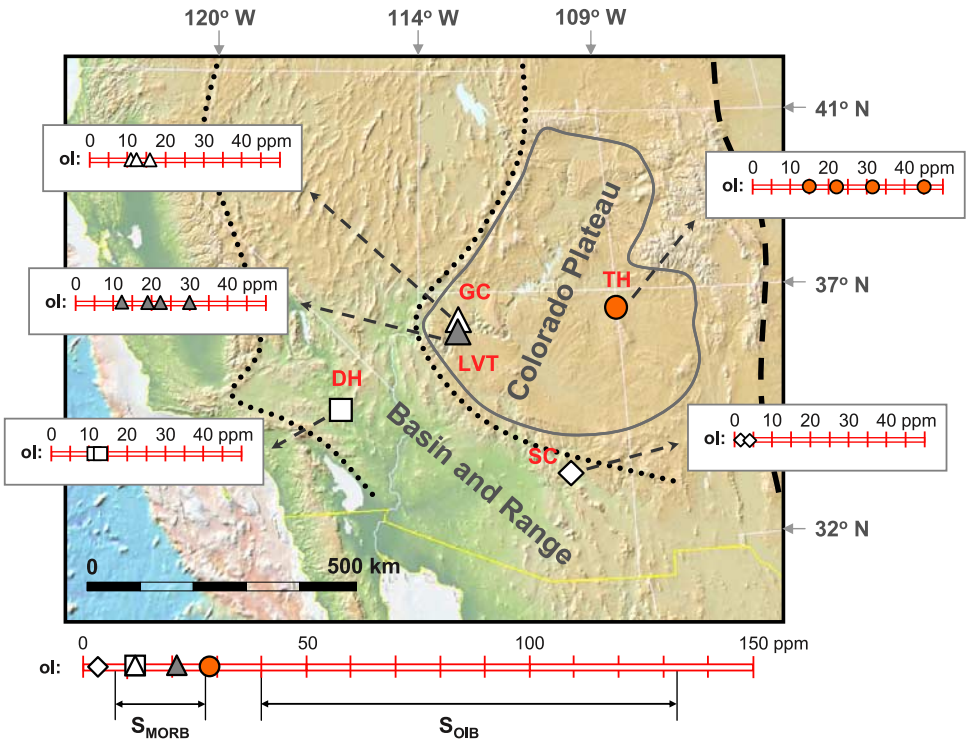

Figure 1. Sample localities and measured water contents (ppm H_2O) in olivine (ol) using FTIR. At the bottom, the average water content in olivine from each sample locality is compared to the inferred olivine water contents for mid-ocean ridge basalt (MORB) mantle source S_{MORB} and the ocean island basalt (OIB) mantle source S_{OIB} whose whole rock water contents were taken from *Hirschmann* [2006]. Olivine water contents of MORB and OIB sources were calculated assuming a peridotite stoichiometry of ~60% olivine, ~30% orthopyroxene, and ~10% clinopyroxene and using the partitioning coefficients of *Aubaud et al.* [2004], revised according to the FTIR-SIMS intercalibration by *Aubaud et al.* [2007]. DH, Dish Hill (open squares); GC, Mount Trumbull (open triangles); LVT, Vulcan's Throne (solid triangles); SC, San Carlos (open diamonds); TH, The Thumb within the Navajo volcanic field (solid circles). Also shown are the outlines for the Basin and Range, the Colorado Plateau, and the estimated eastern limit of Cordilleran orogeny (the dashed black curve) based on topography.

1996; *Hirth et al.*, 2000; *Hirth and Kohlstedt*, 2004; *Pollack*, 1986]. Rock-deforming experiments show that the plastic strength of olivine aggregates dramatically decreases in the presence of H^+ [*Chopra and Paterson*, 1984; *Hirth and Kohlstedt*, 1996; *Kohlstedt et al.*, 1995; *Mackwell et al.*, 1985; *Mei and Kohlstedt*, 2000]. If dehydration does enhance lithospheric strength and ensure longevity, the question that arises is whether cratonic mantle can ever be rehydrated, and if so, whether such rehydration can ultimately lead to weakening or even destabilization of the lithosphere. Is cratonic mantle forever, or can it be recycled?

[3] One place bearing potential for answering the above question lies within the North American Cordillera. Despite the fact that much of this region is underlain by Proterozoic to Archean basement [*Bennett and DePaolo*, 1987], the region has been affected by a ~1500 km wide belt of intracontinental deformation associated with Mesozoic Farallon plate subduction and Cenozoic extension [*Dickinson and Snyder*, 1978; *Dickinson*, 2004; *Humphreys et al.*, 2003; *Saleeby*, 2003]. The Colorado Plateau, being largely undeformed, has for the most part represented an "island" of tectonic stability nestled within the Cordilleran orogenic belt. This suggests that the plateau lithosphere has been rheologically strong. Indeed, calculated equilibration pressures of Eocene-hosted mantle xenoliths indicate that the plateau was once underlain by a cold, refractory root extending to depths of > 150 km, not much thinner (<50 km) than the lithosphere presently underlying the undeformed part of the North American craton beneath the Great Plains to the east [*Ehrenberg*, 1982a, 1982b; *Lee et al.*, 2001b; *Riter and Smith*, 1996; *Smith*, 2000; *West et al.*, 2004]. Thus, the Colorado Plateau's tectonic stability seems to be related to the fact that its underlying mantle root originally had some characteristics of typical stable Archean cratonic mantle. The problem, however, is that seismic studies associated with the RISTRA array [e.g., *West et al.*, 2004; *Wilson et al.*, 2005] suggest that the plateau lithosphere is now between ~120 and ~150 km thick [*West et al.*, 2004] and thus obviously thinned. What allowed the Colorado Plateau lithosphere to be thinned? One hypothesis is that the basal part of the lithosphere was replaced by asthenosphere due to rifting along the Basin and Range province or Rio Grande valley [*West et al.*, 2004]. Another hypothesis is that the lithosphere was hydrated and consequently weakened and thinned [*Dixon et al.*, 2004; *Humphreys et al.*, 2003; *Lee*, 2005]. Introduction of water beneath this region has

Table 1. Water Contents in Minerals and Estimated Mineral Modes[a]

	ol		cpx		opx		spl		grt		WR		
	Weight Percent	ppm H_2O	Weight Percent	ppm H_2O	Weight Percent	ppm H_2O	Weight Percent	ppm H_2O	Weight Percent	ppm H_2O	ppm H_2O	$R_{H_2O}^{ol/cpx}$	$R_{H_2O}^{cpx/opx}$
KBH-1[b]						211 (217)							
BCN201B[b]		7(6.6)		337(342)									
DH98-25	78	13	5	539[c]	15	235	2				73	0.025	2.3
DH98-30	90	11	5	550[c]	3	164[c]	2				42	0.019	3.4
GC2a	85	12	3		10	364[c]	2						
GC2b	55	12	5	520[d]	35	333	5				149	0.023	1.6
GC2c	55	12	3	439[d]	40	326	2				150	0.026	1.3
GC2e	56	16	2	514[d]	40	387	2				174	0.03	1.3
GC2x	76	11	3	559[d]	20	388	1				102	0.019	1.4
LVT-1	83	19	1		15		1						
LVT-2	69	12	3	572[d]	25	402	3				126	0.021	1.4
LVT-3	71	22	5		20	377[c]	4						
LVT-4	73	30	2		20		5						
SC99-1		2		171		82						0.014	2.1
SC99-2	60	4	8	178[c]	30	53	2				32	0.02	3.4
TH1	68	22	1	893[c]	30	274	1				106	0.025	3.3
TH2	89.9	45	0.1	957[c]	10	303					72	0.047	3.2
TH3	88	31	3	793[c]	8				1			0.039	
TH4	94.8	15	0.2	849[c]	4	281[c]			1		27	0.018	3

[a]Mineral modes (in wt %) are estimated by point counting. Whole rock (WR) water contents are reconstructed from measured water contents in minerals and estimated mineral modes. FTIR calibrations follow *Bell et al.* [2003, 1995]. Measured water contents for samples KBH-1 and BCN201B are compared to the originally reported values [*Bell et al.*, 1995; *Peslier and Luhr*, 2006]. Abbreviations are ol, olivine; cpx, clinopyroxene; opx, orthopyroxene; spl, spinel; grt, garnet. $R_{H_2O}^{ol/cpx}$, ratios of olivine water contents to clinopyroxene water contents; $R_{H_2O}^{cpx/opx}$, ratios of clinopyroxene water contents to orthopyroxene water contents.

[b]Samples from previous studies, values in parentheses represent the originally reported water contents [*Bell et al.*, 1995; *Peslier and Luhr*, 2006].

[c]Either A_α or A_β is calculated based on the A_α/A_β ratio of another sample from the same group.

[d]Assuming IR absorbance A_α (with E//a) equals to A_β.

been suggested to have occurred during the late Mesozoic to early Cenozoic when the Farallon plate was undergoing low-angle subduction and may have released slab-derived fluids into the overriding North American lithosphere [*Dixon et al.*, 2004; *Humphreys et al.*, 2003; *Lee*, 2005; *Smith et al.*, 1999; *Smith*, 2000; *Smith et al.*, 2004; *Smith and Griffin*, 2005]. However, most evidence supporting the above rehydration hypothesis come from trace element systematics and the presence of hydrous phases in lavas and a few peridotite and eclogite xenoliths. Few systematic studies exist [e.g., *Bell and Rossman*, 1992; *Grant et al.*, 2007a; *Mosenfelder et al.*, 2006] on actual water contents in mantle xenoliths from western North America [see *Dixon et al.*, 2004] that might provide further insight into rheologic structure and evolution of this region.

[4] This paper presents new evidence for lithospheric mantle hydration with measurements of water in nominally anhydrous minerals (NAMs), such as olivine and pyroxene, in mantle xenoliths from the Colorado Plateau and the surrounding Basin and Range. We then explore issues such as the nature of the hydration fluids and hydration time in the context of regional tectonics and the trace element geochemistry of mantle xenoliths and lavas in western United States. We finally discuss the implications of subduction-induced hydration for the lithospheric evolution of western North America and beyond.

2. Study Area and Sample Description

[5] Seventeen peridotite xenolith samples from five localities representing a ~500 km long transect from of the Mojave Desert to the center of the Colorado Plateau were analyzed (Figure 1).

[6] Samples from the Pliocene Dish Hill alkali basalt cinder cone (DH) in the Basin and Range include one coarse-grained (1 to 3 mm) harzburgite (DH98–25) and one fine-grained (~0.1 to 1 mm) lherzolite (DH98–30). The former is relatively undeformed, but the latter is highly foliated and contains large orthopyroxene porphyroblasts. Both xenoliths are fresh and show no evidence for weathering.

[7] Xenoliths from the Quaternary Grand Canyon Uinkaret volcanic field (on the west margin of the Colorado Plateau) are subdivided into two groups, the Grand Canyon (GC) group (5 samples) and the Vulcan's Throne (LVT) group (4 samples). The GC xenoliths are composed of dominantly coarse-grained (~2 to 6 mm) harzburgites characterized by high modal orthopyroxene content (Table 1); orthopyroxenes commonly show partly resorbed inclusions of olivine [*Smith et al.*, 1999]. The LVT group are also coarse-grained (~1 to 5 mm) harzburgites but are distinctive in that they have a high population of fine-grained spinels.

[8] The two xenolith samples from the Pliocene San Carlos alkali basalt lava flow (SC) just off the south margin of Colorado Plateau in the southern Basin and Range are coarse grained (~1 to 5 mm) harzburgites composed of extremely fresh olivine and pyroxenes.

[9] Another four samples hosted by minettes are from the Eocene [*Roden et al.*, 1988] Navajo volcanic field (TH, Thumb) in the center of the Colorado Plateau, including one garnet lherzolite (TH3), one garnet harzburgite, one spinel lherzolite and one spinel harzburgite. All four Navajo xenoliths show various extents of alteration on mineral

Table 2. Polarized FTIR Absorption for Olivine[a]

	T (μm)	A_α	A_β	A_γ
BCN201B-ol-10-on	360	4		20
BCN201B-ol-15-bxo	359		11	
DH98-25-ol-26-bxo	410		24	31
DH98-25-ol-27-on	369	9		30
DH98-30-ol-4-bxo	171		22	28
DH98-30-ol-9-on	168	6		28
GC2a-ol-10-bxo	254		21	31
GC2a-ol-12-on	184	10		31
GC2b-ol-4-on	472	9		28
GC2b-ol-17-on	452	9		31
GC2b-ol-21-bxo	414		22	32
GC2c-ol-3-bxo	311		21	26
GC2c-ol-11-on	348	7		30
GC2e-ol-15-on	227	12		28
GC2e-ol-21-bxo	340		35	26
GC2x-ol-2-on	305	10		25
GC2x-ol-23-bxo	400		17	28
LVT-1-ol-3-bxo	231		39	34
LVT-1-ol-4-on	259	17		32
LVT-2-ol-5-bxo	400		21	29
LVT-2-ol-26-on	407	11		31
LVT-3-ol-22-on	310	20		43
LVT-3-ol-24-bxo	318		30	45
LVT-4-ol-10-on	171	19		51
LVT-4-ol-12-bxo	171		30	52
SC99-1-ol-5-2-bxo	415		3	6
SC99-1-ol-5-19-on	540	3		5
SC99-2-ol-4-bxo	269		3	10
SC99-2-ol-5-on	272	5		8
TH1-ol-12-on	265	13		45
TH1-ol-19-bxo	335		42	60
TH2-ol-3-bxo	350		46	156
TH2-ol-11-on	372	34		159
TH3-ol-8-bxo	223		35	88
TH3-ol-26-on	214	28		60
TH4-ol-10-on	230	13		37
TH4-ol-25-bxo	180		27	32

[a]T, Grain thickness in μm; A_α, A_β, and A_γ (cm^{-2}), absorbances with the polarization direction parallel to α, β, and γ, respectively.

grain boundaries (indicated by the presences of Fe oxides and/or serpentine) but mineral cores are mostly optically clear and hence largely unaffected by alteration.

3. Methods

3.1. Sample Preparation and Fourier Transform Infrared Spectroscopy Analysis

[10] Central portions of peridotite xenoliths were wrapped in several sheets of paper and gently crushed (to maintain grain integrity). Around 30 grains of olivine, clinopyroxene and orthopyroxene (respectively) from each xenolith sample were handpicked under optical binoculars. Picked mineral grains were ultrasonically bathed in ethanol and dried at temperatures up to 85°C overnight. The mineral grains were subsequently imbedded in epoxy, and doubly polished sections of ~50 to 300 μm thick were prepared by hand polishing using alumina powder (to 0.5 μm fine). After thin sections were cleaned with deionized water and ethanol, the mounted mineral grains were carefully examined under the petrographic microscope to check for fractures and inclusions and to identify crystallographic orientations (based on interference figures). Grains optically free (or with a low population) of fractures and inclusions were chosen. Of these, those that contained surfaces perpendicular to the optic normal (ON), acute bisectrix (Bxa) or obtuse bisectrix (Bxo) directions were identified and their crystallographic orientations were recorded. Grain thicknesses were measured by focusing on each grain's polished surfaces using a petrographic microscope, which was calibrated with a digital micrometer. Before Fourier transform infrared (FTIR) spectroscopy analysis, the mounted sections were again cleaned using deionized water and ethanol, dried up to 85°C overnight, and stored in a tightly sealed desiccator.

[11] Polarized infrared (IR) spectra (absorbance between wave numbers 650 and 4000 cm^{-1}) of each suitably oriented mineral (with the electric vector E parallel to each optical indicatrix index α, β, and γ) were collected in the Department of Earth Sciences at Rice University using a Nicolet 4700 FTIR spectrometer attached to a Continuum Microscope which was equipped with a KBr beam splitter and a ZnSe infrared polarizer. In most cases, 250 scans using an aperture size of 100 × 100 μm were performed during each measurement (500 scans were made for San Carlos olivines because of their low signal to background ratios). To minimize interference from atmospheric H_2O, the IR beam path as well as the sample stage was enclosed in an environmental chamber continuously purged with nitrogen, and a new background spectrum was collected every 10 min. Spectra were normalized to 1 cm thickness and the absorbances from the silicate matrix were manually subtracted using a baseline correction tool built into the Nicolet Omnic© software. The O-H absorption intensities (between 3700 and 3100 cm^{-1} for olivine, 3750 and 3000 cm^{-1} for clinopyroxene, and 3750 and 2800 cm^{-1} for orthopyroxene) were then determined by integrating the area under the baseline-corrected absorbance curves.

[12] Absorbances were converted to water contents (ppm by weight of H_2O) using the Beer-Lambert law in the form $C_{H_2O} = A_i/\mu_i$, where $A_i = A_\alpha + A_\beta + A_\gamma$ is the total absorbance (cm^{-2}) (A_α, A_β and A_γ correspond to the integrated absorbance in the E//α, E//β and E//γ directions, respectively: see Tables 2, 3, and 4 for values of A_α, A_β and A_γ) and μ_i is the molar absorption coefficient (ppm^{-1} cm-2) of 5.3 for olivine, 7.09 for clinopyroxene and 14.84 for orthopyroxene [*Bell et al.*, 1995, 2003]. When not enough suitably oriented grains are available (which was often the case for clinopyroxene and occasionally for orthopyroxene due to their rarities), either A_α or A_β was calculated using the A_α/A_β of samples from the same group or by assuming $A_\alpha \sim A_\beta$ (see Table 1 for details). Such approximations are justified by the fact that pyroxenes often have similar absorptions along the α and β directions [*Bell et al.*, 1995; *Peslier et al.*, 2002; *Skogby et al.*, 1990].

[13] Uncertainty in grain orientations is estimated to be ±5°, which converts to ~±5% uncertainties in measured water contents. Uncertainty on grain thickness measurements is ±2%. Baseline correction was carried out using subjective identification of the baseline, so quantification of the uncertainty is somewhat ambiguous. However, by comparing net absorbances of repeated baseline corrections on a given spectrum, we estimate the baseline correction uncertainty to be ±5% for olivine from all sample localities except for San Carlos. The low water contents in San Carlos olivines resulted in very low O-H absorbances, which are only slightly distinguishable from background

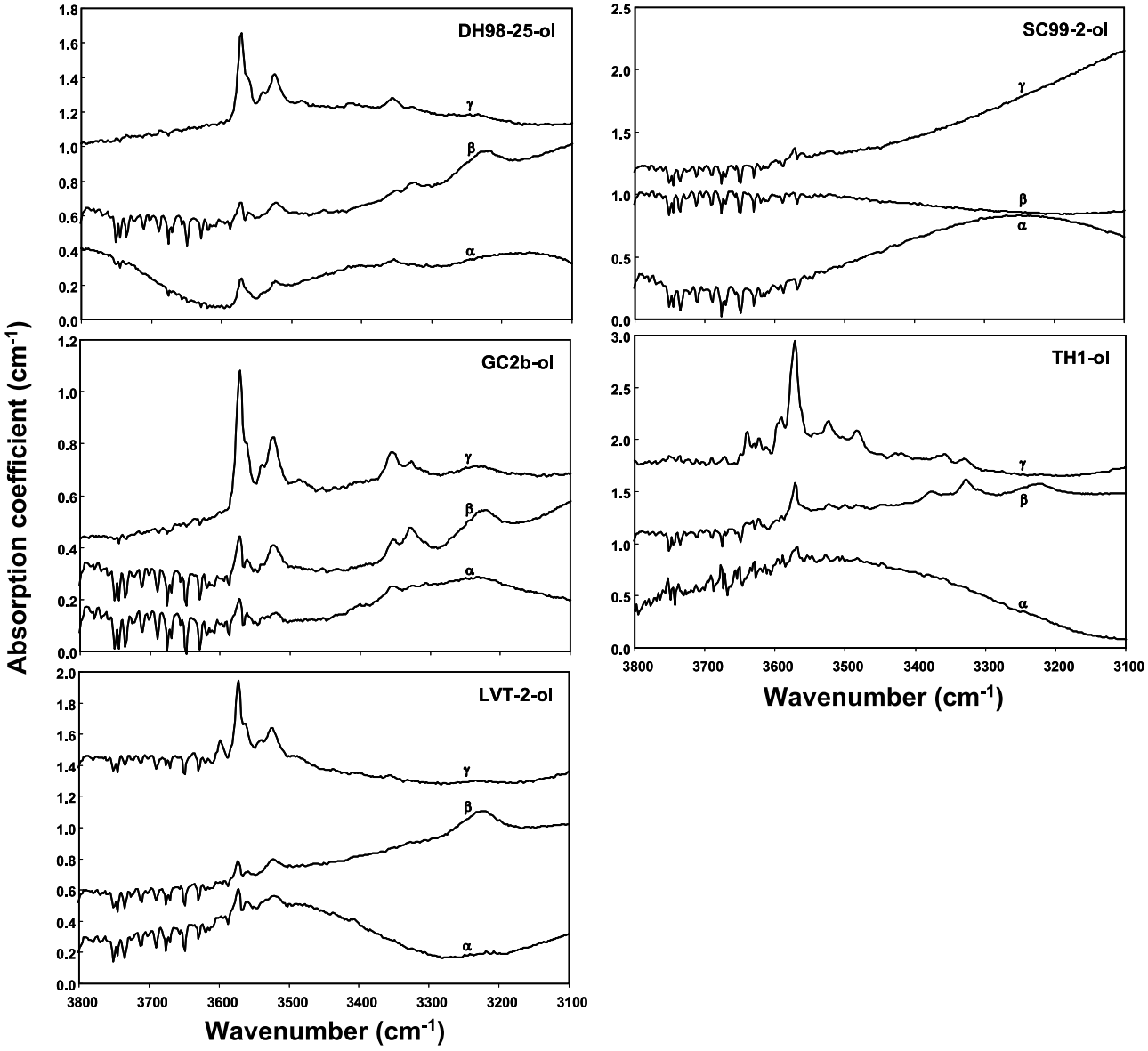

Figure 2. Polarized IR absorption spectra for olivine (ol) normalized to 1 cm thickness; spectra for different orientations (α, β, and γ) are offset for clarity. Sample names (sample name-ol) are shown at the top right corner of each panel.

(Figure 2); the resulting uncertainty from baseline correction for San Carlos olivines was thus ±20%. For the pyroxenes, the estimated uncertainties associated with baseline correction, serpentine peak subtraction (manually subtracting O-H peaks caused by serpentine, refer to discussion in section 5.2 and Table 3 for details) and the estimation of unmeasured absorbance (refer to Table 1) add up to ±10% of net absorbance. Adding the reported uncertainties in the IR calibrations (6% for olivine [*Bell et al.*, 2003] and 10 to 20% for the pyroxenes [*Bell et al.*, 1995]), the total uncertainties on water contents are estimated to be ±12% (1σ) (for non-San Carlos samples) and ±20% (1σ) (for San Carlos samples) for olivine and ±15 to 25% (1σ) for orthopyroxene and clinopyroxene (calculated using the ''addition in quadrature'' error propagation method [*Taylor*, 1997]). The accuracy of our measurements was confirmed by good agreement between our water measurements on previously studied samples (KBH-1 from *Bell et al.* [1995]; BCN201B from *Peslier and Luhr* [2006]) and the reported values in the literature (Table 1).

3.2. Electron Microprobe Analysis

[14] Major and minor element compositions of olivine, clinopyroxene, orthopyroxene and garnet (mineral modes estimated by point counting are listed in Table 1) were analyzed at the University of Houston using an electron microprobe (JEOL JXA-8600) with an accelerating voltage of 15 kV and a beam current of 30 nA. The counting time was set to be 50 s for most elements. For each mineral phase, core to rim compositions of 3 to 5 mineral grains

Table 3. Polarized FTIR Absorption for Clinopyroxene[a]

	T (μm)	A_α	A_β	A_γ
BCN201B-cpx-7-bxo	297		772	844
DH98-25-1-cpx-4-bxo	312		1321	1001
DH98-30-cpx-16-on	318	1530		1023
GC2b-cpx-6-bxo	303		1326	1036
GC2c-cpx-27-bxo	234		1115	885
GC2e-cpx-15-bxo	216		1302	1038
GC2x-cpx-13-bxo	254		1424	1118
LVT-2-cpx-19-bxo	306		1445	1144
SC99-1-cpx-11-bxo	278		422	343
SC99-1-cpx-41-bxa	240	444	413	
SC99-2-cpx-19-bxo	350	478		350
TH1-cpx-23-bxo	277		2046	2538
TH2-cpx-2-on	80	3100		3027
TH3-cpx-4-bxo	115		1477	1940
TH4-cpx-19-bxo	242		1590	2206
TH1-cpx-23-bxo[b]	277		1635	2178
TH2-cpx-2-on[b]	80	2700		2332
TH3-cpx-4-bxo[b]	115		1438	1940
TH4-cpx-19-bxo[b]	242		1552	2071

[a]T, Grain thickness in μm; A_α, A_β, and A_γ (cm^{-2}), absorbances with the polarization direction parallel to α, β, and γ, respectively.
[b]Serpentine peaks were subtracted.

were measured (>4 measurements per grain). For major elements (>1 wt. %), the accuracy and precision of measurements are better than 1%.

4. Results

4.1. Mineral Chemistries and Thermobarometry

[15] Other than exsolution lamellae of clinopyroxene in orthopyroxene from one Dish Hill sample (DH98−30) and the corona textures of garnet from the 2 Navajo xenoliths, no obvious intra or intergranular heterogeneities were observed (refer to standard deviations in Table 5). Mineral chemistries (grain averaged) from electron microprobe analyses are listed in Table 5 (clinopyroxene lamella and garnet corona compositions are not included). Mg # (100 × Mg/(Mg+Fe) in molar compositions) of olivines range from 90.6 to 92.2 for Navajo, 90.0 to 91.6 for Grand Canyon, 89.7 to 90.5 for Dish Hill, and ~89.4 for San Carlos (based on sample SC99−2).

[16] Pyroxene and garnet mineral chemistries were used to calculate temperatures and pressures of equilibration. For spinel peridotites, temperatures were estimated using the two pyroxene thermometers of *Wells* [1977] and *Brey and Köhler* [1990] (for the latter, 1.5 GPa was assumed) (Table 6). For the two garnet peridotites (TH3 and TH4), pressures and temperatures of equilibration were simultaneously estimated (Table 6) using the two-pyroxene thermometers and the barometer of *Brey and Köhler* [1990], which is based on Al in orthopyroxene coexisting with garnet. Temperatures were also estimated on the basis of Ca content in orthopyroxene using the calibration of *Brey and Köhler* [1990] (assuming 1.5 GPa when garnet is missing) and listed in Table 6 for comparison. Despite discrepancies in temperatures estimated by different thermometers, xenoliths from the center of the Colorado Plateau and San Carlos consistently record higher equilibration temperatures (~950 to 1200°C) than those from the southern Basin and Range (~850 to 1050°C) and the west margin of the plateau (~600 to 950°C) (Table 6). Equilibration pressures calculated for the 2 garnet peridotites TH3 and TH4 are ~3.5 and 3.7 GPa, respectively (Table 6).

4.2. FTIR Results

[17] Selected spectra of O-H absorbances for olivine, clinopyroxene, and orthopyroxene are plotted in Figures 2, 3, and 4, respectively. For olivine, O-H absorption bands are mainly restricted to band group I, 3450 to 3650 cm^{-1} [*Bai and Kohlstedt*, 1993]. Group II bands between 3200 and 3450 cm^{-1} [*Bai and Kohlstedt*, 1993] are also occasionally observed but with much lower intensities (Figure 2). Spectra for clinopyroxenes (Figure 3) and orthopyroxenes (Figure 4) show O-H absorptions at similar wave numbers as reported by *Bell et al.* [1995]. Absorption peaks associated with serpentine minerals [*Miller et al.*, 1987; *Mosenfelder et al.*, 2006] are present at ~3680 cm^{-1} in spectra of clinopyroxenes and orthopyroxenes (of lower intensities) from Navajo xenoliths (TH, Figures 3 and 4). From these spectra, water contents were calculated to be 11 to 13 ppm in olivine, 539 to 550 ppm in clinopyroxene, and 164 to 235 ppm in orthopyroxene for samples from Dish Hill (DH); 11 to 16 ppm in olivine, 439 to 559 ppm in clinopyroxene, and 326 to 388 ppm in orthopyroxene for GC group from Grand Canyon; 12 to 30 ppm in olivine, 572 ppm in clinopyroxene, and 402 to 377 ppm in orthopyroxene for LVT group from Grand Canyon; 2 to 4 ppm in olivine, 171 to 178 ppm

Table 4. Polarized FTIR Absorption for Orthopyroxene[a]

	T (μm)	A_α	A_β	A_γ
KBH-1-opx-4-bxo	368		653	1279
KBH-1-opx-6-on	382	1202		1278
DH98-25-opx-9-bxo	351		978	1381
DH98-25-opx-27-on	323	1122		1400
DH98-30-opx-17-bxo	165		700	966
GC2a-opx-5-bxo (off)	412		1366	2379
GC2b-opx-5-bxo	323		1051	1909
GC2b-opx-13-on	313	1536		2197
GC2c-opx-26-on	382	1428		2096
GC2c-opx-29-bxo	359		1315	2060
GC2e-opx-9-on (off)	340	1791		2437
GC2e-opx-10-bxo	400		1472	2477
GC2x-opx-11-bxo	404		1479	2480
GC2x-opx-26-on (off)	321	1791		2486
LVT-2-opx-14-on	366	1770		2839
LVT-2-opx-17-on	267	1810		2824
LVT-2-opx-26-bxo	387		1396	2758
LVT-3-opx-26-on	270	1820		2505
SC99-1-opx-1-4-on	627	303		665
SC99-1-opx-1-7-bxo	663		251	658
SC99-2-opx-9-bxa	412	194	168	
SC99-2-opx-20-on	386	184		421
TH1-opx-1-on	404	1392		2078
TH1-opx-26-bxo	275		791	2047
TH2-opx-5-on	282	1210		2303
TH2-opx-26-bxo	240		1047	2263
TH4-opx-16-bxo	295		1113	2210
TH1-opx-1-on[b]	404	1318		1988
TH1-opx-26-bxo[b]	275		753	2021
TH2-opx-5-on[b]	282	1210		2303
TH2-opx-26-bxo[b]	240		1031	2257
TH4-opx-16-bxo[b]	295		965	2103

[a]T, grain thickness (μm); A_α A_β, and A_γ (cm^{-2}), absorbances with the polarization direction parallel to α, β, and γ, respectively. "Off" indicates the orientation of the thin section is slightly off from the given optical direction (such as On, Bxa, or Bxo).
[b]Serpentine peaks were subtracted.

Table 5. Compositions of Minerals Measured by Electron Microprobe[a]

	DH98-25		DH98-30		GC2a		GC2b		GC2c		GC2e		GC2x		LVT-1		LVT-2		LVT-3		LVT-4		SC99-2		TH1		TH2		TH3		TH4	
Olivine																																
SiO_2	40.65	±0.12	40.46	±0.11	40.56	±0.09	40.24	±0.23	40.53	±0.11	40.19	±0.13	39.81	±0.26	40.79	±0.45	40.28	±0.05	40.22	±0.27	40.58	±0.09	40.13	±0.21	40.52	±0.18	41.12	±0.16	40.07	±0.22	41.01	±0.13
Al_2O_3	0.01	±0.01	0.01	±0.00	0.00	±0.00	0.01	±0.01			0.01	±0.01	0.01	±0.00			0.01	±0.01	0.01	±0.00			0.02	±0.00	0.01	±0.00	0.02	±0.01	0.02	±0.01	0.02	±0.01
Cr_2O_3					0.01	±0.00			0.01	±0.00	0.01	±0.00	0.01	±0.00											0.03	±0.00	0.05	±0.01	0.04	±0.01	0.06	±0.01
FeO	9.23	±0.11	9.96	±0.10	8.22	±0.09	9.54	±0.08	9.64	±0.12	9.74	±0.12	8.92	±0.13	7.84	±0.12	8.72	±0.03	9.69	±0.11	9.13	±0.07	10.23	±0.13	7.68	±0.10	7.83	±0.08	8.99	±0.13	8.21	±0.06
MnO	0.14	±0.01	0.15	±0.01	0.13	±0.01	0.14	±0.01	0.15	±0.01	0.15	±0.01	0.13	±0.02	0.12	±0.01	0.14	±0.01	0.15	±0.01	0.14	±0.01	0.16	±0.01	0.11	±0.01	0.12	±0.01	0.11	±0.01	0.12	±0.01
NiO	0.42	±0.01	0.40	±0.02	0.41	±0.02	0.40	±0.01	0.41	±0.01	0.43	±0.02	0.40	±0.01	0.43	±0.01	0.41	±0.01	0.40	±0.01	0.43	±0.01	0.41	±0.01	0.44	±0.01	0.43	±0.02	0.41	±0.01	0.44	±0.02
MgO	49.37	±0.08	48.77	±0.15	50.21	±0.34	49.21	±0.24	48.97	±0.15	49.24	±0.10	48.76	±0.17	50.62	±0.47	48.77	±0.31	49.05	±0.44	49.55	±0.14	48.30	±0.42	51.12	±0.26	50.72	±0.32	48.35	±0.15	50.36	±0.23
CaO	0.06	±0.00	0.05	±0.01	0.04	±0.00	0.05	±0.00	0.04	±0.00	0.06	±0.00	0.04	±0.00	0.02	±0.00	0.03	±0.00	0.03	±0.00	0.03	±0.01	0.07	±0.00	0.05	±0.00	0.05	±0.00	0.07	±0.00	0.07	±0.00
Na_2O																											0.01	±0.01	0.02	±0.01	0.01	±0.01
Total	99.89		99.79		99.57		99.60		99.76		99.83		98.09		99.84		98.35		99.55		99.87		99.32		99.97		100.34		98.07		100.29	
Clinopyroxene																																
SiO_2	51.62	±0.28	52.05	±0.47	53.30	±0.32	52.15	±0.23	53.44	±0.35	52.25	±0.27	52.14	±0.32	54.92	±0.32	52.71	±0.26	52.92	±0.32	53.70	±0.28	50.98	±0.28	53.07	±0.26	52.62	±0.32	53.79	±0.34	53.43	±0.39
TiO_2	0.38	±0.06	0.54	±0.02			0.11	±0.01	0.04	±0.01	0.12	±0.01	0.08	±0.01	0.01	±0.00	0.15	±0.02	0.11	±0.01	0.06	±0.01	0.55	±0.02			0.40	±0.19	0.22	±0.01	0.09	±0.09
Al_2O_3	6.29	±0.44	6.12	±0.23	1.71	±0.11	3.98	±0.19	3.33	±0.13	4.39	±0.13	4.43	±0.21	1.30	±0.27	3.01	±0.21	2.80	±0.16	1.84	±0.12	8.76	±0.19	1.52	±0.01	1.81	±0.79	4.15	±0.04	2.50	±0.05
Cr_2O_3	0.77	±0.06	0.68	±0.03	0.32	±0.06	0.44	±0.07	0.41	±0.07	0.43	±0.06	0.43	±0.09	0.30	±0.03	0.18	±0.05	0.20	±0.01	0.21	±0.03	0.65	±0.05	0.84	±0.02	1.87	±0.21	1.41	±0.04	1.51	±0.05
FeO	2.66	±0.05	2.59	±0.04	2.04	±0.04	2.46	±0.05	2.51	±0.06	2.70	±0.04	2.55	±0.07	1.68	±0.05	2.13	±0.06	2.34	±0.06	2.07	±0.06	3.12	±0.06	2.15	±0.03	2.50	±0.08	3.20	±0.05	2.68	±0.06
MnO	0.09	±0.01	0.09	±0.01	0.08	±0.01	0.09	±0.02	0.09	±0.01	0.10	±0.01	0.08	±0.01	0.06	±0.01	0.08	±0.01	0.09	±0.01	0.08	±0.01	0.09	±0.01	0.08	±0.01	0.09	±0.01	0.10	±0.01	0.10	±0.01
NiO	0.05	±0.01	0.04	±0.01	0.05	±0.02	0.06	±0.01	0.05	±0.02	0.05	±0.02	0.04	±0.01	0.05	±0.02	0.04	±0.02	0.03	±0.01	0.04	±0.01	0.04	±0.01	0.07	±0.01	0.06	±0.01	0.08	±0.01	0.06	±0.02
MgO	15.39	±0.18	15.32	±0.14	17.87	±0.08	16.75	±0.13	16.99	±0.10	16.62	±0.10	16.36	±0.11	17.55	±0.23	16.89	±0.14	16.71	±0.15	17.62	±0.10	14.38	±0.14	17.12	±0.09	17.26	±0.54	16.66	±0.18	17.65	±0.34
CaO	20.57	±0.27	21.89	±0.15	24.54	±0.10	23.59	±0.11	23.39	±0.07	23.04	±0.13	22.50	±0.08	24.48	±0.02	23.31	±0.11	23.48	±0.18	24.99	±0.10	20.61	±0.12	22.07	±0.11	20.28	±0.77	18.02	±0.12	19.40	±0.53
Na_2O	1.30	±0.12	1.36	±0.06	0.29	±0.02	0.59	±0.03	0.56	±0.02	0.74	±0.03	0.45	±0.02	0.18	±0.01	0.11	±0.01	0.11	±0.01	0.09	±0.010	1.37	±0.02	0.42	±0.01	1.34	±0.39	1.76	±0.02	0.90	±0.04
Total	99.12		100.69		100.19		100.22		100.80		100.44		99.06		100.51		98.61		98.79		100.71		100.55		97.35		98.25		99.38		98.34	
Orthopyroxene																																
SiO_2	55.24	±0.26	55.94	±0.40	56.39	±0.37	55.14	±0.21	56.18	±0.46	55.05	±0.34	55.22	±0.20	58.28	±0.25	55.64	±0.49	55.72	±0.43	56.58	±0.34	54.62	±0.18	56.20	±0.30	55.92	±0.22	56.25	±0.45	56.29	±0.23
TiO_2	0.06	±0.01	0.09	±0.02			0.03	±0.01	0.01	±0.01	0.03	±0.01	0.02	±0.01			0.05	±0.01	0.04	±0.01	0.02	±0.01	0.12	±0.01			0.10	±0.01	0.10	±0.01	0.03	±0.01
Al_2O_3	4.18	±0.09	3.82	±0.17	2.01	±0.10	3.81	±0.08	3.40	±0.09	4.11	±0.11	4.53	±0.14	1.53	±0.21	3.47	±0.58	3.97	±0.13	2.58	±0.14	6.15	±0.06	1.55	±0.02	1.53	±0.02	2.26	±0.06	2.00	±0.04
Cr_2O_3	0.33	±0.01	0.29	±0.03	0.30	±0.05	0.36	±0.02	0.35	±0.02	0.34	±0.02	0.38	±0.03	0.29	±0.07	0.19	±0.05	0.22	±0.02	0.19	±0.04	0.31	±0.01	0.49	±0.01	0.65	±0.02	0.41	±0.01	0.67	±0.01
FeO	5.93	±0.10	6.24	±0.16	5.24	±0.08	5.96	±0.06	6.15	±0.07	6.10	±0.09	6.09	±0.08	5.13	±0.05	5.81	±0.1	6.44	±0.12	5.97	±0.09	6.67	±0.08	4.67	±0.09	4.75	±0.06	5.69	±0.09	5.10	±0.08
MnO	0.15	±0.02	0.16	±0.01	0.13	±0.01	0.15	±0.01	0.16	±0.01	0.16	±0.01	0.15	±0.02	0.14	±0.01	0.16	±0.01	0.16	±0.01	0.16	±0.01	0.16	±0.01	0.12	±0.01	0.12	±0.02	0.12	±0.01	0.13	±0.01
NiO	0.10	±0.01	0.09	±0.02	0.11	±0.02	0.11	±0.03	0.10	±0.01	0.12	±0.01	0.10	±0.01	0.08	±0.02	0.09	±0.02	0.08	±0.02	0.09	±0.01	0.11	±0.01	0.12	±0.01	0.12	±0.01	0.13	±0.01	0.13	±0.01
MgO	32.89	±0.12	32.91	±0.63	34.79	±0.13	33.18	±0.16	33.42	±0.17	33.00	±0.12	32.27	±0.13	34.47	±0.08	32.86	±0.32	32.30	±0.32	34.22	±0.15	30.64	±0.18	32.53	±0.23	33.75	±0.20	31.82	±0.22	32.75	±0.10
CaO	0.68	±0.01	0.96	±0.73	0.54	±0.02	0.66	±0.01	0.63	±0.01	0.72	±0.01	0.59	±0.01	0.41	±0.17	0.45	±0.02	0.44	±0.01	0.42	±0.02	0.84	±0.01	0.76	±0.01	0.90	±0.04	1.06	±0.05	1.03	±0.03
Na_2O	0.06	±0.01	0.06	±0.03	0.01	±0.01	0.03	±0.01	0.02	±0.01	0.04	±0.00	0.01	±0.01	0.01	±0.04							0.07	±0.01	0.01	±0.01	0.16	±0.01	0.20	±0.01	0.09	±0.00
Total	99.61		100.57		99.53		99.42		100.42		99.67		99.35		100.34		98.72		99.38		100.23		99.69		96.45		97.99		98.04		98.21	
Garnet																																
SiO_2																													41.89	±0.14	42.10	±0.28
TiO_2																													0.29	±0.01	0.17	±0.02
Al_2O_3																													21.41	±0.22	19.70	±0.09
Cr_2O_3																													2.10	±0.13	3.65	±0.21
FeO																													6.91	±0.10	6.31	±0.08
MnO																													0.30	±0.01	0.32	±0.02
NiO																													0.01	±0.01	0.01	±0.01
MgO																													19.49	±0.08	18.84	±0.28
CaO																													4.89	±0.07	6.34	±0.03
Na_2O																													0.04	±0.01	0.02	±0.00
Total																													97.33		97.46	

[a]The measured compositions (in wt % oxide) and the corresponding standard deviations (1σ) are given for each sample.

Table 6. Calculated Equilibration Temperatures and Pressures for Xenoliths[a]

Label	T_{Wells} (°C)	T_{BKN}[b](°C)	P_{BKN} (GPa)	$T_{Ca\_In\_opx}$[b] (°C)
DH98-25	965	998		961
DH98-30	861	840		1042
GC2a	733	589		913
GC2b	807	714		957
GC2c	874	814		944
GC2e	856	796		976
GC2x	950	920		931
LVT-1	832	726		854
LVT-2	929	876		878
LVT-3	912	846		872
LVT-4	746	601		860
SC99-2	973	1005		1011
TH1	965	950		993
TH2	984	1005		1030
TH3	1096	1206	3.5	1160
TH4	1112	1193	3.7	1154

[a] T_{Wells}, temperatures calculated using two pyroxene thermometer of *Wells* [1977]; T_{BKN}, temperatures calculated using two pyroxene thermometer of *Brey and Köhler* [1990]; $T_{Ca\_In\_Opx}$, temperature calculated on the basis of Ca content in orthopyroxene according to *Brey and Köhler* [1990]; P_{BKN}, pressure calculated on the basis of Al in orthopyroxene coexisting with garnet according to *Brey and Köhler* [1990].

[b] Equilibrium pressure of 1.5 GPa is used when garnet is not present.

in clinopyroxene, and 53 to 82 ppm in orthopyroxene for xenoliths from San Carlos (SC); and 15 to 45 ppm in olivine, 793 to 957 ppm in clinopyroxene, and 274 to 303 ppm in orthopyroxene for xenoliths from Navajo (TH) (Table 1). The following maximum intragrain heterogeneities (the contrasts between core and rim) were found in olivine water contents for all but San Carlos (SC) xenoliths: ~40% for DH, ~40% for GC, ~60% for LVT, and ~20% for TH. The maximum intergrain heterogeneities in olivine water contents (based on the cores of different mineral grains) are: ~3% for DH, ~14% for GC, ~7% for LVT, ~22% for SC, and ~38% for TH.

[18] No intragrain heterogeneities (e.g., zonation) in water contents were found in either clinopyroxene or orthopyroxene, and the intergrain heterogeneities are in general subtle (<10% in most cases) for orthopyroxene. Not enough measurements are available for clinopyroxene (due to its rarity) to assess the intergrain heterogeneities. In Figures 5a and 5b, the above listed water contents, representing the highest measured values when intergrain heterogeneities occurred, were further compared to water contents in alkali basalt-hosted mantle xenoliths from other regions: Kilbourne Hole, New Mexico [*Grant et al.*, 2007a]; Washington [*Peslier et al.*, 2002; *Peslier and Luhr*, 2006]; Chile [*Demouchy et al.*, 2006]; and Mexico [*Peslier et al.*, 2002; *Peslier and Luhr*, 2006]. With the exception of San Carlos (SC), most of our samples have higher water contents than these localities.

5. Discussion

5.1. Depleted Lithospheric Mantle Beneath the Colorado Plateau

[19] Olivine Mg # calculated on the basis of microprobe measurements (Table 5) ranges from 90 to 92.2 for xenoliths from the Colorado Plateau (Grand Canyon and Navajo) and from 89.4 to 90.5 for xenoliths off the Colorado Plateau (San Carlos and Dish Hill). The spatial variations in olivine Mg # are consistent with results of previous studies suggesting that the Colorado Plateau has a more depleted mantle root than its surroundings [*Lee et al.*, 2001b; *Smith*, 2000]. The high orthopyroxene modes and the presence of resorbed olivine inclusions as documented in Grand Canyon xenoliths (the GC group, Table 1) were also reported by *Smith et al.* [1999] in their study of xenoliths from the Colorado Plateau and were interpreted as products of orthopyroxene growth during water-rock interactions due to aqueous fluid infiltration into the mantle wedge on the dehydration of the subducting Farallon slab during late Mesozoic to early Cenozoic.

5.2. Representativeness of Water Content in Xenoliths

[20] Measurements of water in mantle xenoliths provide a direct way to probe the water content in the lithospheric mantle provided that the water in mantle xenoliths is not changed during magma ascent or surface exposure. We discuss each of these provisions below.

5.2.1. On the Disturbance of Water Content During Postemplacement Weathering

[21] The extrapolation of experimental diffusion data [*Woods et al.*, 2000; *Hercule and Ingrin*, 1999; *Ingrin et al.*, 1995; *Mackwell and Kohlstedt*, 1990; *Stalder and Skogby*, 2003] to surface *P-T* conditions indicates that after emplacement hydrogen diffusion in NAMs is extremely slow and thus no significant water exchange between xenoliths and the environment can occur over reasonable geologic timescales. Consequently, diffusive contamination from meteoric water during weathering processes is unlikely to penetrate deeply beyond grain boundary zones. We also note that the calculated water solubilities in NAMs by extrapolating the solubility equation given by *Kohlstedt et al.* [1996] to surface *P-T* conditions are much lower than the water contents measured in our study. Chemical reactions, however, can still result from reaction of water of meteoric origin with NAMs, generating new hydrous phases on grain boundaries. Although we picked alteration-free mineral grains to the best of our ability, one exception is in Navajo xenoliths where intact clinopyroxene and orthopyroxene grains were scarce and small so that microfractures were sometimes unavoidable during FTIR analysis. In such samples, absorption peaks at ~3680 cm^{-1} associated with the presences of submicroscopic serpentine minerals [*Miller et al.*, 1987; *Mosenfelder et al.*, 2006] were occasionally observed in the spectra (Figure 3). These serpentine bands, however, were carefully excluded from integration by manually subtracting the serpentine peaks during baseline correction.

5.2.2. Issue of Water Loss/Gain During Magma Ascent

[22] The entrainment of mantle xenoliths by ascending magma can be accompanied by water exchange between mantle xenoliths and the host magma due to the rapid diffusion of hydrogen in NAMs at elevated temperature as predicted by hydrogen diffusion experiments [e.g., *Mackwell and Kohlstedt*, 1990]. The entrainment process, however, is typically accompanied by water loss from xenoliths rather than water gain. Water loss is often manifested by H diffusion profiles across mineral grains, a phenomenon so far having only been observed in olivines [e.g., *Demouchy et al.*, 2006; *Peslier and Luhr*, 2006]. Diffusive water loss may be caused by the fact that the

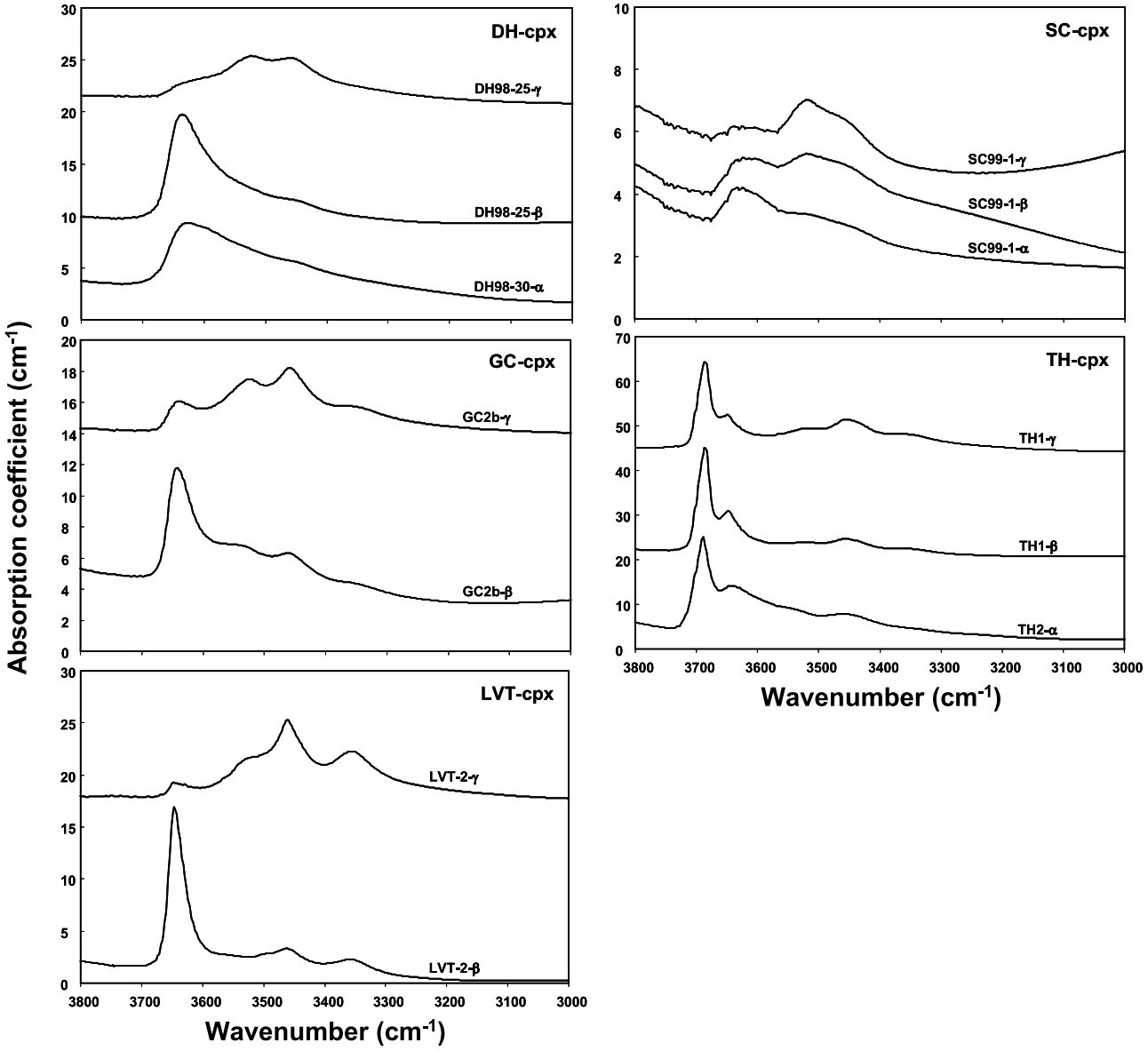

Figure 3. Polarized IR absorption spectra for clinopyroxene (cpx). Normalized to 1 cm thickness and offset for clarity. Labels above each spectrum are sample names and polarization directions (sample name-polarization).

transporting magma is generally undersaturated in water and the solubility of water in NAMs (except for Al-saturated enstatite [*Mierdel et al.*, 2007]) decreases substantially with decreasing pressure [*Bai and Kohlstedt*, 1992; *Woods et al.*, 2000; *Demouchy et al.*, 2006; *Hercule and Ingrin*, 1999; *Ingrin et al.*, 1995; *Ingrin and Skogby*, 2000; *Mackwell and Kohlstedt*, 1990; *Peslier and Luhr*, 2006; *Stalder and Skogby*, 2003]. Apart from San Carlos, all xenoliths (particularly those from the Colorado Plateau) are exceptionally enriched in water compared to mantle xenoliths derived from other localities of similar tectonic settings, including Kilbourne Hole, New Mexico [*Grant et al.*, 2007a]; Washington [*Peslier et al.*, 2002; *Peslier and Luhr*, 2006]; Chile [*Demouchy et al.*, 2006]; and Mexico [*Peslier et al.*, 2002; *Peslier and Luhr*, 2006] (Figures 5a and 5b). Also plotted in Figures 5a and 5b are lines representing equilibrium ratios of water between olivine and pyroxene based on experimentally determined water partition coefficients of *Aubaud et al.* [2004] and the revised values according to the new FTIR-SIMS calibrations in *Aubaud et al.* [2007]. The deviation to low values of measured water contents in olivine from that predicted by equilibrium partitioning suggests that some water might have been preferentially lost from olivine compared to pyroxene in most xenoliths samples (Figure 5a). This is also illustrated by comparing the measured water contents in olivine with those calculated to be in equilibrium with the measured clinopyroxene and orthopyroxene water contents using various partition coefficients from the literature [*Aubaud et al.*, 2004, 2007; *Grant et al.*, 2007b] (Figures 6a, 6b, and 6c).

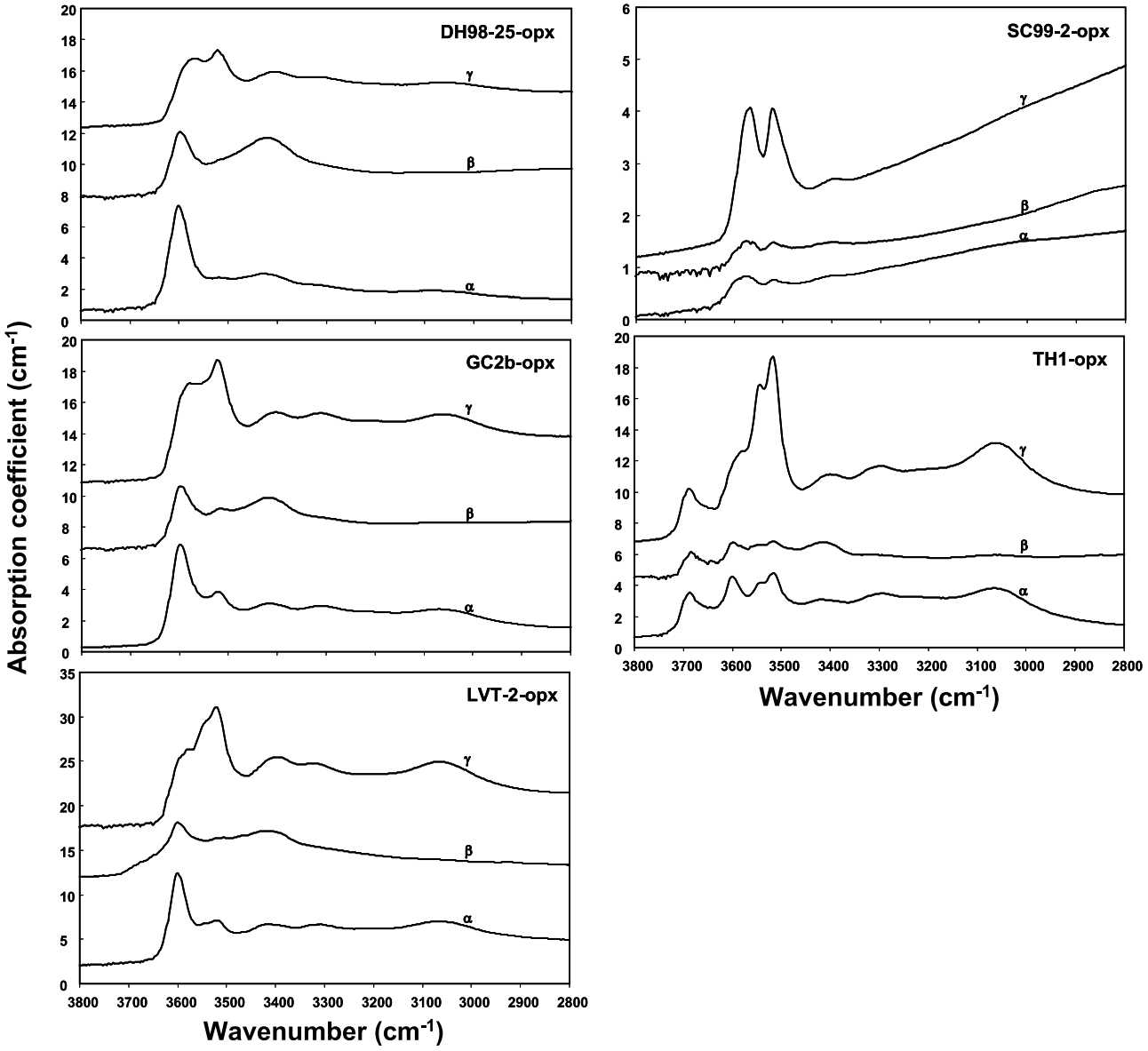

Figure 4. Polarized IR absorption spectra for orthopyroxene (opx). Normalized to 1 cm thickness and offset for clarity. Polarization directions (α, β, and γ) are labeled above each spectrum and sample names (sample name-opx) are shown at the top right corner of each panel.

[23] Water loss from olivine was further indicated by the observation that the majority of analyzed olivines show zonation (Figure 7 and Table 7), with decreasing water content (as indicated by O-H absorption) toward the rims, consistent with water loss during transport via hydrogen diffusion. Such diffusive loss is likely due either to a drop in fluid pressure (and thus solubility of water in olivine) during magma ascent or to partitioning of water into the magma [*Kohlstedt and Mackwell*, 1998; *Mackwell and Kohlstedt*, 1990]. Experimental studies have quantified two water-loss mechanisms in olivine. One involves a rapid initial loss of some hydrogen due to proton-polaron exchange in which protons are lost from the mineral and the ferric-ferrous iron ratio increases; this is rate limited by self-diffusion of hydrogen. A second scenario involves a slower process where defect associates comprising protons and metal vacancies are lost; this is rate limited by the diffusion of the metal vacancies [*Kohlstedt and Mackwell*, 1998]. The first mechanism allows only partial dehydration, as olivine can only accommodate a small percentage of iron as ferric. Thus, while some hydrogen may be lost rapidly, complete loss of water requires the second mechanism, which is consistent with the observation of hydroxyl retained in olivines in xenoliths. The first mechanism is also operative in pyroxenes, while the latter mechanism, though likely, has yet to be quantified.

5.2.3. Minimum Estimate of Prexenolith Entrainment Water Contents and Comparison to Mid-ocean Ridge Basalt and Ocean Island Basalt Mantle Sources

[24] In order to determine preeruptive or preentrainment water contents of the mantle xenoliths, the amount of water

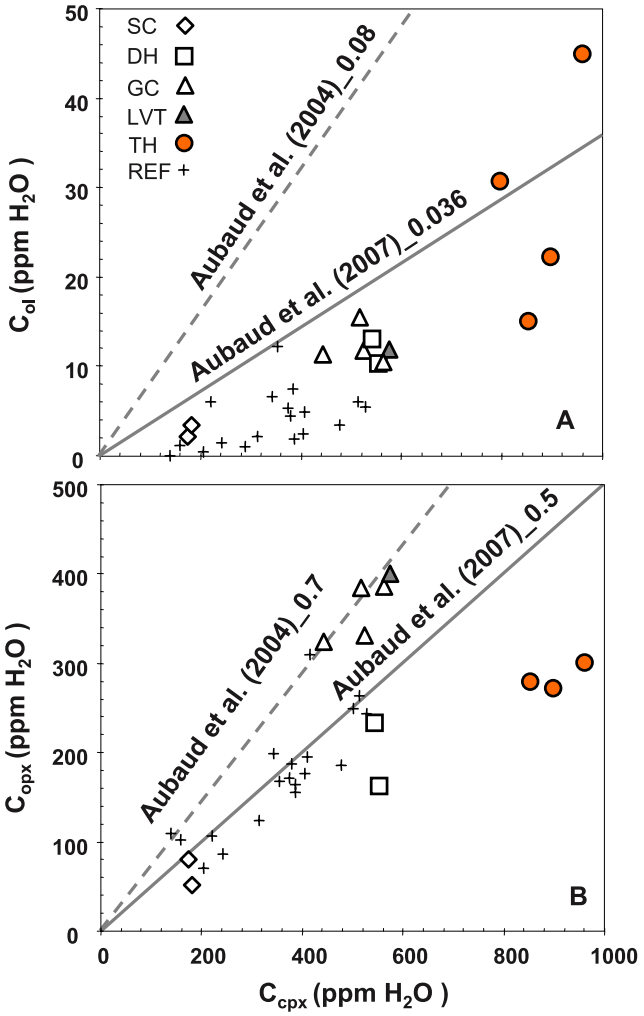

Figure 5. Measured water contents in minerals compared to literature data and experimental constraints. (a) Water contents in olivine plotted against water contents in clinopyroxene. (b) Water contents in orthopyroxene plotted against water contents in clinopyroxene. Literature data (the crosses, labeled REF) contain measurements on alkali basalt-hosted xenoliths from Kilbourne Hole, New Mexico [*Grant et al.*, 2007a]; Washington [*Peslier et al.*, 2002; *Peslier and Luhr*, 2006]; Chile [*Demouchy et al.*, 2006]; and Mexico [*Peslier et al.*, 2002; *Peslier and Luhr*, 2006]. The olivine water content (56 ppm H_2O) of the one plotted Chile sample [*Demouchy et al.*, 2006] lies out of Figure 5a. The dashed lines represent the partition coefficients of *Aubaud et al.* [2004], and the solid lines are the revised partition coefficients according to the new calibration of *Aubaud et al.* [2007]. Numbers after the references are the values of the used partition coefficients.

loss during magma ascent needs to be determined, but so far there are no reliable means of doing so. We therefore consider the measured mineral water contents (Figures 5a and 5b and Table 1) to represent minimum estimates of the prexenolith entrainment water contents. We have reconstructed the whole rock water contents using our measured values and they should also be taken as minimum estimates (Table 1).

[25] To put the measured xenolith water contents into context, we have plotted the olivine water contents (the average value) for each sample locality along with the inferred water contents for olivines in equilibrium with the mid-ocean ridge basalt (MORB) mantle sources (~7 to 27 ppm H_2O) and the ocean island basalt (OIB) mantle sources (~40 to 133 ppm H_2O) (Figure 1). As we will discuss later, our choice of using olivine rests on the assumption that mantle rheology is controlled primarily by olivine. The water content for olivines in equilibrium with the MORB mantle source were calculated from the estimated whole rock water contents of ~50–200 ppm H_2O for the MORB source [*Danyushevsky et al.*, 2000; *Dixon et al.*, 2002; *Hirschmann*, 2006; *Michael*, 1988; *Saal et al.*, 2002; *Simons et al.*, 2002] and applying the mineral/mineral partition coefficients of *Aubaud et al.* [2004] (revised according to *Aubaud et al.* [2007] where $D_{H_2O}^{ol/cpx}$ ~ 0.036 and $D_{H_2O}^{ol/opx}$~ 0.072), assuming a peridotite stoichiometry of 60% olivine, 30% orthopyroxene and 10% clinopyroxene. The water contents for olivines in equilibrium with the OIB sources were similarly calculated from the inferred whole rock water contents of ~300–1000 ppm for the OIB mantle source [*Dixon et al.*, 1997; *Dixon et al.*, 2002; *Hauri*, 2002; *Hirschmann*, 2006; *Jamtveit et al.*, 2001; *Nichols et al.*, 2002; *Seaman et al.*, 2004; *Wallace et al.*, 2002]. We note that the partition coefficients we used in these calculations ($D_{H_2O}^{ol/cpx}$~ 0.036 and $D_{H_2O}^{ol/opx}$ ~ 0.072) differ slightly from those reported by *Hauri et al.* [2006] ($D_{H_2O}^{ol/cpx}$~ 0.067 and $D_{H_2O}^{ol/opx}$ ~ 0.083 on average). The inconsistency in measured water partition coefficients is a complicated issue and is beyond the scope of this study. Calculations using partition coefficients of *Aubaud et al.* [2004] (revised according to *Aubaud et al.* [2007]) indicate that all but San Carlos xenoliths analyzed in our study have olivine water contents as high as or higher than that estimated for various asthenospheric mantle sources (Figure 1). The highest water contents were found in the Navajo (TH) xenoliths from the Colorado Plateau, which plot beyond the higher end of the inferred water content for the MORB source (Figure 1).

5.2.4. How Representative of the Lithosphere Are Our Water Measurements?

[26] An important question is whether the high water contents measured here are representative of the lithospheric mantle or whether they are associated with xenoliths derived from a narrow zone in or at the base of the lithosphere. For those xenoliths from the Colorado Plateau, thermobarometry on the garnet-peridotites indicate depth ranges up to ~140 km (Figure 8b). These xenoliths give equilibration temperatures of ~1200°C, which indicates that they are well within the lithosphere and that the base of the lithosphere is at greater depths.

[27] Although the pressures of equilibration for garnet-free peridotites cannot be calculated, a rough estimate can be determined from the depths corresponding to their temperatures and the xenolith geotherm. Equilibration temperatures for the spinel peridotites (TH, GC and LVT groups) range from ~800 to 1000°C (T_{BKN} in Table 6; note that we excluded four anomalously low temperatures be-

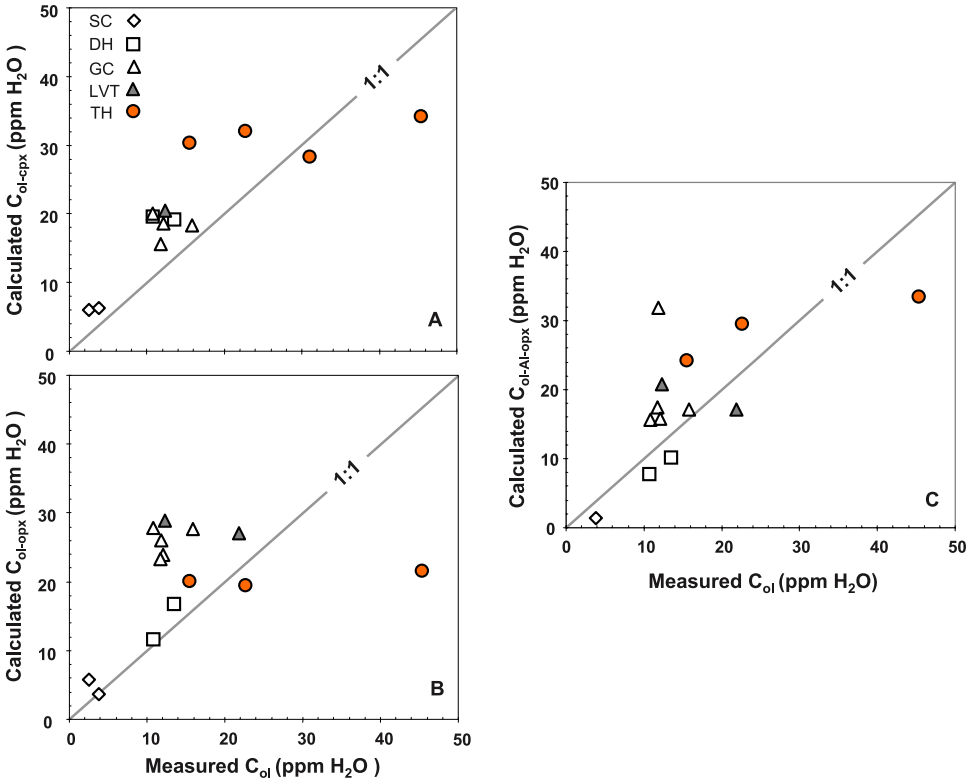

Figure 6. Measured water contents in olivine compared to calculated values using experimentally determined partition coefficients. (a) Calculated water contents for olivine based on water contents in clinopyroxene $C_{ol\text{-}cpx}$ versus measured water contents in olivine C_{ol}. (b) Calculated water contents for olivine based on water contents in orthopyroxene $C_{ol\text{-}opx}$ versus measured water contents in olivine C_{ol}. (c) Calculated water contents for olivine based on water contents in orthopyroxene using Al content-dependent partition coefficient $C_{ol\text{-}Al\text{-}opx}$ versus measured water contents in olivine C_{ol}. The partition coefficients $D_{H_2O}^{ol/cpx}$ and $D_{H_2O}^{ol/opx}$ used in Figures 6a and 6b are after *Aubaud et al.* [2004] revised according to the FTIR-SIMS intercalibration by *Aubaud et al.* [2007]. The used partition coefficient in Figure 6c, $D_{H_2O}^{ol/opx}$, is calculated using Al content-dependent partition coefficient for orthopyroxene $D_{H_2O}^{opx/melt}$ after *Grant et al.* [2007b] and partition coefficient for olivine $D_{H_2O}^{ol/melt}$ given by *Aubaud et al.* [2004] revised according to the calibration by *Aubaud et al.* [2007]. The 1 to 1 line is shown for reference.

cause of lack of agreement between the different thermometers), which corresponds to a depth range between 70 to 90 km (Figure 8b). This combined with the depth range of the garnet peridotites indicates that Colorado Plateau xenoliths derive from depths between ~70 and 140 km. Taking the geotherm that passes through the *P-T* points of our xenoliths and those from previous studies for the Colorado Plateau, we find that the lithosphere at the time these xenoliths were sampled (30–40 Ma) was >150 km thick (Figure 8b). Because all of the samples have high relatively high water contents, the implication is that the hydrated nature of the lithosphere is possibly pervasive, at least on a vertical scale.

[28] The next section discusses possible hypotheses for the origin of these high water contents. Such high water contents are intriguing because the high Mg # in olivine and low clinopyroxene mode of many of the xenoliths represent clear evidence that they have experienced significant melt depletion (>10%). Because water behaves incompatibly during melting [e.g., *Dixon et al.*, 1988; *Michael*, 1995, 1988], we would have expected these xenoliths to have been initially dry.

5.3. Rehydration of North American Lithosphere

5.3.1. A Case for Recent Rehydration

[29] Has the western North American lithospheric mantle been wet since its stabilization? The elevated water contents in our xenoliths seem to be inconsistent with their melt-depleted nature as indicated by their high olivine Mg # (mostly between ~90 and 92). In fact, the most depleted lithospheric mantle underlies the central Colorado Plateau and yet its xenoliths (Mg #*s* ~ 91 to 92) appear to be the wettest (~45 ppm H_2O in olivines). The high water content of the Colorado Plateau lithospheric mantle, as recorded in mantle xenoliths, is also inconsistent with its preservation as a thick lithosphere for billion year timescales because a wet lithospheric mantle is not rheologically strong enough to resist asthenospheric flow (see below). The alternative hypothesis is that the North American lithospheric mantle, particularly that beneath the tectonically quiescent Colorado Plateau, has recently been rehydrated. A number of investigators have suggested that much of the lithospheric mantle beneath western North America could have been hydrated by fluids released during prograde metamorphism from a

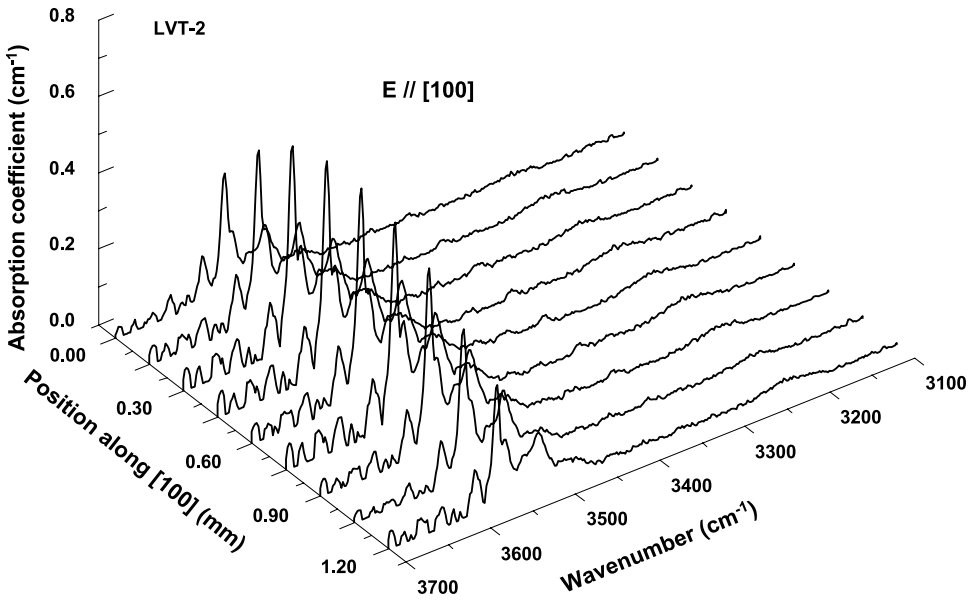

Figure 7. FTIR spectra across an olivine grain from xenolith LVT-2. The profile was collected from edge to edge along the [100] axis (with E//[100]) at 150 μm interval. Spectra are normalized to 1 cm thickness and baseline corrected.

shallowly subducting Farallon plate between ~80 and 35 Ma [*English et al.*, 2003; *Humphreys et al.*, 2003; *Lee*, 2005; *Smith*, 1995; *Smith et al.*, 1999, 2004; *Smith and Griffin*, 2005]. The requirements of this hypothesis are twofold: first, there must be enough water in the Farallon slab to serve as a source of fluids, and second, enough of this water must be retained long enough in the slab to reach distances of ~800 km inboard from the trench. A number of studies now suggest that extensive portions of subducting oceanic slab may be serpentinized [*Lee and Chen*, 2007; *Li and Lee*, 2006; *Ranero et al.*, 2003]. Faults, fracture zones, and cracks provide ready conduits for the introduction of seawater deep into oceanic lithosphere, resulting in hydrothermally altered zones around the cracks. While the depth to which water can penetrate is a question of debate, it has been suggested that serpentinization can extend as deep as ~40 km in relatively old and cold lithosphere [*Li and Lee*, 2006]. Indeed, the Farallon slab at the trench ~80 Ma ago was old (>50 Ma [*Engebretson et al.*, 1985; *English et al.*, 2003]), which means that the thermal state was sufficiently cool to permit extensive serpentinization. Thermal modeling of the flat subducting Farallon slab indicate that the slab surface will dehydrate first while the slab interior (e.g., the serpentinized core of the slab) will heat up more slowly so that dehydration of the interior serpentinite is delayed long enough for water to be transported ~800 km inboard of the trench, far enough to reach the Colorado Plateau [*English et al.*, 2003].

5.3.2. Xenolith Petrology and Trace Element Arguments for the Rehydration Hypothesis

[30] Rehydration of the Colorado Plateau lithospheric mantle was inferred from detailed petrologic studies of xenoliths. For example, some plateau mantle xenoliths have excess orthopyroxene or chlorite, best explained by the passage of silica-rich fluids [*Smith*, 1995]. In addition, garnetite xenoliths found on the central Colorado Plateau have been suggested to represent the products of rodingite-like mantle metasomatism with the fluids derived from dehydration of serpentine [*Smith and Griffin*, 2005]. Xenolith trace element data are also consistent with this hypothesis. Progressing inboard from the west coast toward the Colorado Plateau, *Lee* [2005] noted that the trace element signature of metasomatic fluids evolves with distance. Close to the trench (e.g., beneath the extinct Sierran arc), mantle xenoliths are enriched in the fluid-mobile elements, Sr, Pb, U, Ba, and Cs, but not in fluid immobile elements, such as the rare earth elements (REEs) and the high field strength elements (HFSEs = Nb, Ta, Zr, Hf). This suggests that near the trench temperatures were not high enough to cause significant silicate melting, which would have released the REEs and HFSEs.

[31] In contrast, although the Navajo mantle xenoliths from the Colorado Plateau are also enriched in fluid-mobile elements, they are unlike the near-trench xenoliths as they are enriched in Pb, U, Ba, and Cs, but not Sr [*Lee*, 2005]. They are also enriched in the light REEs (LREEs) and HFSEs although La is still more enriched than Nb resulting in the low Nb/La ratios attributed to subduction-related fluids [*Lee*, 2005]. Interestingly Sr is depleted compared to the middle REEs (in the near trench xenoliths, there is positive Sr anomaly) [*Lee*, 2005]. *Lee* [2005] suggested that the plateau xenoliths have been metasomatized by a hydrous melt from the basaltic oceanic crust that had been previously dehydrated of its fluid-mobile elements near the trench. In such a scenario, fluids released from the serpentinite core of the slab rise up through the already dehydrated oceanic crust causing partial melting. The trace element signature of the resulting hydrous melt inherits the serpentinite signature and that of the dehydrated basalt. Thus, the REEs and HFSEs derive from the basalt, whereas the fluid-mobile elements derive from the serpentinized core of the slab. Recent studies of serpentinites indicate enrichments in

Table 7. FTIR Absorption Profile Along [100] Direction for Selected Olivine Grains[a]

D (μm)	A_γ
DH98-25	
0	23
25	23
125	28
225	34
325	31
425	26
525	23
575	22
DH98-30	
0	19
100	23
220	28
340	23
440	21
GC2a	
0	29
200	31
400	31
600	31
800	31
1000	26
1200	24
1325	21
GC2c	
0	18
200	23
400	24
600	26
800	25
1000	20
1200	18
LVT-2	
0	15
150	21
300	25
450	28
600	29
750	26
900	24
1050	19
1200	16
TH1	
0	51
150	60
350	60
550	60
750	49
TH2	
0	137
100	143
400	156
700	148
1000	137
TH3	
0	79
150	80
300	85
450	86
600	88
750	86
900	86
1050	83
1200	83

[a]D, distance (μm) measured from edge to edge of given grain along the [100] direction; $A\gamma$ (cm^{-2}), absorbance with the polarization direction parallel to γ.

these same fluid-mobile elements with the exception of Sr [*Li and Lee*, 2006]. As a result, serpentinizing fluids do not contribute Sr to the dehydrating fluids and the resultant hydrous melt inherits the negative Sr anomaly of the basalt. All of these observations suggest that much of the North American lithosphere as far eastward as the Colorado Plateau was metasomatized and that the metasomatizing agent was likely a fluid (or hydrous melt) from beneath the Colorado Plateau.

5.3.3. Timing Arguments for the Rehydration Hypothesis

[32] When did such metasomatism occur? The flat subduction of the Farallon plate beneath the North America occurred between ~80 to 35 Ma [*English et al.*, 2003; *Humphreys et al.*, 2003; *Lee*, 2005; *Smith*, 1995; *Smith et al.*, 1999, 2004; *Smith and Griffin*, 2005]. U-Pb ages of zircons from metasomatic veins in Colorado Plateau lithospheric mantle range from ~80 to 65 Ma [*Smith and Griffin*, 2005]. Moreover, the evolution of the trace element signature with distance from the trench associated with fluids coming off of a slab undergoing prograde metasomatism suggests that the metasomatic events beneath the Colorado Plateau and the Sierra Nevada may be related to the same subduction system. Collectively, these observations provide circumstantial evidence that subduction of the Farallon plate during the late Cretaceous through early Cenozoic may have hydrated the North American lithosphere.

5.3.4. A Wet North American Lithosphere

[33] The water contents measured in our xenoliths collected across western North America provide direct evidence that the lithosphere beneath the Colorado Plateau is now wet. Together with petrologic and geochemical data described above, a strong case for Cenozoic rehydration of North American lithosphere can be made, but a perplexing feature of our water data is that the central part of the plateau appears to have higher water contents than regions to the west (Dish Hill and Grand Canyon) (Figure 1), apparently contradicting the general notion that water release should decrease with distance from the trench [*Kelly et al.*, 2006]. In other words, more water should have been introduced into the lithospheric mantle beneath the Basin and Range than beneath the central Colorado Plateau (Figure 1). However, postsubduction tectonic environment in western North America may have altered the subduction imprints. The physiographic region known as the Basin and Range has undergone significant mid to late Cenozoic extension [*Wernicke*, 1992] which likely resulted in decompression melting of the base of the lithosphere and the underlying asthenosphere [*Daley and DePaolo*, 1992; *Wang et al.*, 2002]. Such melting could have extracted ("redepleted") some or all of the subduction-introduced water in the lithosphere. The mid-Cenozoic ignimbrite flare-up in the region now underlain by the Basin and Range could have been the manifestation of melting the hydrated lithospheric mantle [*Humphreys et al.*, 2003; *Lipman*, 1992]. In contrast, the extent of lithospheric thinning beneath the Colorado Plateau was apparently less than that beneath the Basin and Range [*Wernicke*, 1992], resulting in less decompressional melting. This would allow subduction-introduced water and trace elements to be better retained beneath the plateau.

5.4. On the Effect of Water on Lithospheric Mantle Rheology

[34] The implications of rehydrating continental lithospheric mantle for the dynamic evolution of the deep lithosphere beneath the Colorado Plateau are discussed in 2 parts: 1) the role of water in controlling the rheology of olivine, the dominant mineral (>60%) in the upper mantle, and 2) the effective viscosity change of the lithospheric mantle beneath the Colorado Plateau after rehydration, which is constrained by the combination of an updated parameterization of the effect of water on the olivine flow law with estimates of the thermal state of the plateau lithosphere.

5.4.1. Creep Behavior of Olivine

[35] Most studies of mantle rheology have focused on olivine, the dominant mineral in the upper mantle [*Hirth and Kohlstedt*, 1996; *Hirth and Kohlstedt*, 2004; *Karato and Wu*, 1993; *Kohlstedt et al.*, 1995]. The flow law for dislocation creep of olivine aggregates is given by *Mei and Kohlstedt* [2000] as

$$\dot{\varepsilon} = A_{cre}\tau^{n_1} f_{H_2O}^{r} \exp\left(-\frac{Q + PV_{cre}}{RT}\right), \quad (1)$$

where A_{cre}, n_1, and r are experimentally determined constants; $\dot{\varepsilon}$ and τ are shear strain rate and shear stress; Q and V_{cre} are the activation energy and activation volume for dislocation creep of olivine; and P, T, and R are pressure, temperature, and the universal gas constant, respectively. The water fugacity f_{H_2O} was introduced to account for the effect of water on viscosity [*Mei and Kohlstedt*, 2000]. Water fugacity is a thermodynamic parameter that describes the activity of water in a given system (at low pressures, this converges to the partial pressure of water) and is hence a function of temperature and pressure in addition to the water content of the system. During rock deformation experiments, water fugacity is generally adjusted by changing the confining pressure under water-saturated run conditions. Controlling olivine water contents in undersaturated conditions is difficult in experiments, and measuring water contents on small experimental charges is challenging. Under saturated conditions, water fugacity is simply related to pressure and temperature by the equation of state (EOS) of water, making it convenient for experimentalists to constrain.

[36] Water fugacity, however, is not a convenient parameter for those interested in tracking water content in the mantle via petrologic studies or geodynamic models because the mantle is believed to be undersaturated in water [e.g., *Hirschmann*, 2006]. In undersaturated conditions, the water content of olivines can be measured, but the water fugacity must be calculated or inferred assuming thermodynamic equilibrium. A more applicable expression of equation (1) for geodynamicists and petrologists who study

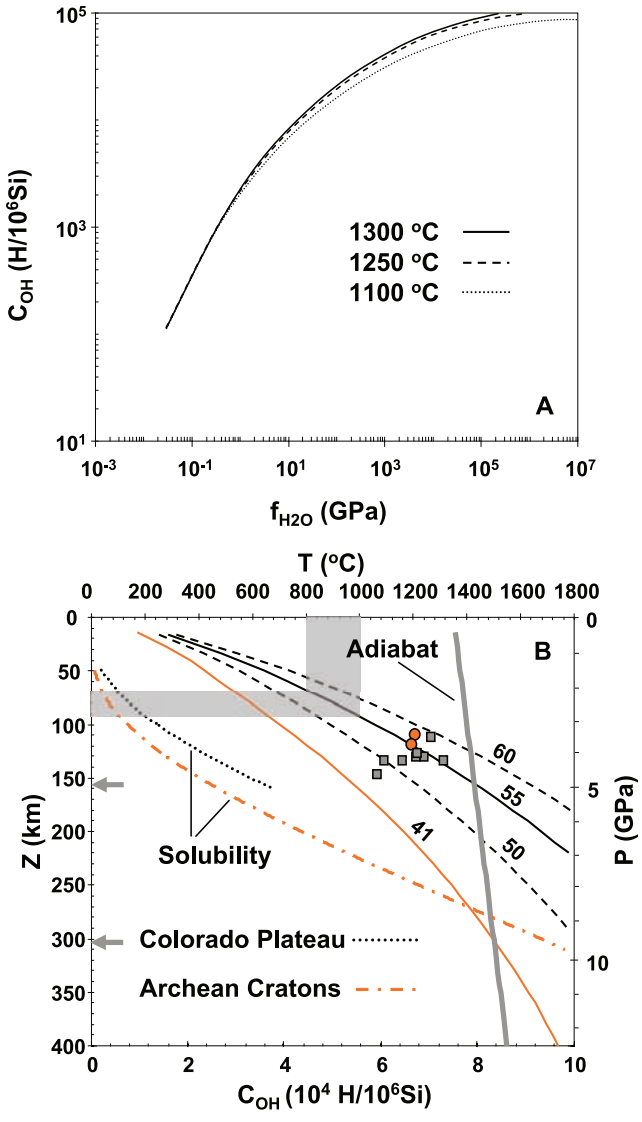

Figure 8. (a) Calculated water solubility in olivine C_{OH} at various temperatures according to equation (2) [*Kohlstedt et al.*, 1996]. (b) Geotherms beneath the Colorado Plateau and Archean cratons and estimated water solubility in olivine. Geotherms for the Colorado Plateau (of various surface heat flows 50, 55, and 60 mW m^{-1}) are calculated for a crustal thickness of 50 km and using the heat production distribution suggested by *Rudnick et al.* [1998]. The equilibration temperatures and pressures (T_{BKN} and P_{BKN} in Table 6) for the two garnet-bearing Navajo xenoliths (circles) are plotted together with literature *P-T* estimates for mantle xenoliths (squares) from the same area [*Ehrenberg*, 1982a]. Geotherm for Archean cratons (heat flow of 41 mW m^{-2} [*Rudnick et al.*, 1998]) is calculated for a crustal thickness of 41 km and using the same heat production distribution [*Rudnick et al.*, 1998]. Water solubilities in olivines following the geotherms (surface heat flow of 55 mW m^{-2} is assumed for the Colorado Plateau) are calculated according to equation (2) [*Kohlstedt et al.*, 1996] with updated IR calibration [*Bell et al.*, 2003]. Mantle adiabat corresponds to a mantle potential temperature of 1350°C [*Asimow et al.*, 2001; *Kinzler and Grove*, 1992; *McKenzie and Bickle*, 1988; *Presnall et al.*, 2002] and a gradient of 0.5°C km^{-1} [*Fei*, 1995; *Navrotsky*, 1995]. The arrows denote the depths at which the adiabat intersects the adopted geotherms. Shaded regions bracket the equilibrium temperatures (T_{BKN} with anomalously low temperatures being dropped) and the corresponding depths (following the 55 mW m^{-2} geotherm) from which on-plateau spinel-bearing xenoliths (TH, GC, and LVT groups) were derived.

Table 8. Parameters Used by the Flow Law and f_{H_2O} - C_{OH} Conversion

Parameter	Value
A_{cre}[a]	1600 MPa$^{-(n_1+r)}$ s^{-1}
Q[a]	520 kJ mol^{-1}
V_{cre}[a]	22 × 10^{-6} m^3 mol^{-1}
n_1[a]	3.5
r[a]	1.2
$A(T)_{hyd}$[b]	1.1 H (10^6 Si)$^{-1}$ MPa^{-1}
V_{hyd}[b]	10.6 × 10^{-6} m^3 mol^{-1}
n_2	1

[a]Values suggested by *Hirth and Kohlstedt* [2004].
[b]Values at 1100°C [*Kohlstedt et al.*, 1996].

natural rocks is obtained by reformulating equation (1) in terms of water concentration C_{OH} (atomic H/10^6 Si; this can be readily converted into ppm by weight H_2O for known mineral composition) in olivines. The use of C_{OH} instead of f_{H_2O} also makes sense as water is, in general, neither lost nor gained in the deep convective mantle system. While some exchange of water may occur between mineral species due to changes in partitioning coefficients with pressure and temperature, to a first order, the water contents of mineral grains are expected to remain relatively constant. If the regulation on creep behavior by water depends only on C_{OH}, then the resulting parameterization of the term documenting the effect of water (to replace the f_{H_2O} term in equation (1) becomes general and should only depend on C_{OH}. Following this line of reasoning, we turn to water solubility experiments run at water-saturated conditions [*Bai and Kohlstedt*, 1992; *Kohlstedt et al.*, 1996]. At water saturation, the water content of olivine C_{OH} (in H/10^6 Si) correlates with the water fugacity f_{H_2O} in the environment following the equation

$$C_{OH} = A(T)_{hyd} f_{H_2O}^{n_2} \exp\left(-\frac{PV_{hyd}}{RT}\right), \quad (2)$$

where V_{hyd} is the activation volume for H^+ incorporation into olivine, n_2 and the preexponential term $A(T)_{hyd}$ are experimentally determined [*Kohlstedt et al.*, 1996]. At first glance, combining equations (2) and (1) results in a modified form of the flow law, wherein f_{H_2O} is substituted with a new term composed of C_{OH} as well as P and T. However, doing so would violate the previous notion that if C_{OH} remains constant the effect of water on creep behavior is constant regardless of changes in temperature and pressure. To avoid such complications, we chose to modify equation (1) by calculating the relationship between f_{H_2O} and C_{OH} for the specific P-T conditions of the rheologic experiments of *Mei and Kohlstedt* [2000]. Using the values of $A(T)_{hyd}$ and V_{hyd} (Table 8) constrained by solubility experiments at 1100°C [*Kohlstedt et al.*, 1996], empirical C_{OH} - f_{H_2O} relations at various temperatures (1100, 1250, and 1300°C) can be calibrated (Figure 8a, f_{H_2O} was calculated according to the equation of state (EOS) for water [*Pitzer and Sterner*, 1994; *Sterner and Pitzer*, 1994]). The C_{OH} - f_{H_2O} relations remain very similar over this temperature range (Figure 8a). Considering that the experimental temperatures used in parameterizing the flow law were mostly ~1250°C [*Mei and Kohlstedt*, 2000], the empirical C_{OH} - f_{H_2O} correlation at 1250°C

$$\ln f_{H_2O} = c_0 + c_1 \ln C_{OH} + c_2 \ln^2 C_{OH} + c_3 \ln^3 C_{OH}, \quad (3)$$

was used to convert f_{H_2O} to C_{OH} in equation (1) (Figure 8a) with $c_0 = -7.9859$, $c_1 = 4.3559$, $c_2 = -0.5742$. $c_3 = 0.0337$, and f_{H_2O} in MPa and C_{OH} in H/10^6 Si. The parameters in equation (3) take into account the new FTIR calibrations of *Bell et al.* [2003] which correct for the systematic error associated with nonpolarized IR calibrations [*Paterson*, 1982] by multiplying nonpolarized determinations of water [*Kohlstedt et al.*, 1996] by a factor of 3.5. Inserting equation (3) into equation (1) finally gives an updated and more convenient form of the flow law by *Mei and Kohlstedt* [2000]

$$\dot{\varepsilon} = A_{cre}\tau^{n_1}\left[\exp\left(c_0 + c_1 \ln C_{OH} + c_2 \ln^2 C_{OH} + c_3 \ln^3 C_{OH}\right)\right]^r \exp\left(-\frac{Q + PV_{crp}}{RT}\right). \quad (4)$$

Although this flow law was parameterized for temperatures around 1250°C, it should be broadly applicable to temperatures from around 1100 to at least 1400°C.

[37] Another way of expressing equation (4) is to incorporate solubility experiments (e.g., equation (2)) directly into the flow law (equation (1)). For example, using the solubility data of *Zhao et al.* [2004], *Hirth and Kohlstedt* [2004] expressed with the flow law in terms of water content C_{OH} by

$$\dot{\varepsilon} = A_{HK}\tau^{n_1} C_{OH}^r \exp\left(-\frac{Q_{HK} + PV_{HK}}{RT}\right), \quad (5)$$

where A_{HK} = 20 MPa$^{-n_1}$H/10^6 Si^{-r} S^{-1} (note that we have updated the value of this constant according to the recent IR calibrations of *Bell et al.* [2003]), Q_{HK} = 480 kJ mol^{-1}, V_{HK} = 11 × 10^{-6} m^3 mol^{-1}, and all other parameters are the same as those used in equation (4). For all intents and purposes, equation (4) and the updated version of equation (5) yield identical results (Figure 9d).

5.4.2. Thermal Structure Beneath the Colorado Plateau

[38] In addition to water, pressure and temperature also play an important role in controlling viscosity (equation (4)). Consequently, the thermal state of the lithosphere needs to be known to fully constrain its rheology. Equilibration pressures (P_{BKN} in Table 6) and temperatures (T_{BKN} in Table 6) of mantle xenoliths from the Colorado Plateau [*Ehrenberg*, 1982b; this study] as constrained by thermobarometry [*Brey and Köhler*, 1990; *Brey et al.*, 1990] are plotted in Figure 8b, as well as model steady state geotherms for different surface heat flows using the distribution of radioactive heat generation suggested by *Rudnick et al.* [1998]. The model geotherms that best fit the thermobarometric data fall between 50 and 60 mW m^{-2}, which is consistent with the measured surface heat flows in the region [*Lee et al.*, 2001b; *Sass et al.*, 1994; *Smith and Griffin*, 2005]. Because model geotherms depend strongly on the distribution of heat production, which is poorly constrained, there is no unique model geotherm for a given

surface heat flow, hence the consistency observed between model and observation may in part be fortuitous. Nevertheless, for our purpose, it is sufficient to simply pick the curve that best fits the xenolith data and use it as an approximation of the thermal state of the lithosphere. The thickness of the lithosphere is estimated by extrapolating this geotherm to higher temperatures until it intersects with the mantle adiabat assumed to represent the base of the lithosphere (assuming an average mantle potential temperature of 1350°C). For comparison, a representative geotherm for Archean cratons calculated in similar way was also plotted (Figure 8b), which was constructed by fitting to xenolith thermobarometric data and a surface heat flow of 41 mW m^{-2} [*Rudnick et al.*, 1998]. Water solubility (in olivine) curves (Figure 8b) were compiled using the geotherms of both the Colorado Plateau (taking surface heat flow of 55 mW m^{-2}) and Archean Cratons, $A(T)_{hyd}$ and V_{hyd} (Table 8) given by *Kohlstedt et al.* [1996], and f_{H_2O} according to *Pitzer and Sterner* [1994] and *Sterner and Pitzer* [1994]. The horizontal shaded region in Figure 8b roughly represents the depths of which those on-plateau xenoliths (TH, GC, and LVT groups) were derived on the basis of their equilibration temperatures T_{BKN} (~600 to 1200°C, Table 6) and following the 55 mW m^{-2} geotherm.

5.5. Effective Viscosities Beneath the Plateau

[39] Combined with water contents in olivines of mantle xenoliths (Figure 1) and geotherms plotted in Figure 8b, equation (4) was used to calculate the shear strain rates $\dot{\varepsilon}$ of the lithospheric mantle beneath the Colorado Plateau at various shear stresses, 0.1, 0.3 and 1 MPa [*Hirth and Kohlstedt*, 2004] (Figure 9a). The effective viscosities η_{eff}, defined as $\eta_{eff} = \tau/\dot{\varepsilon}$, were then plotted in Figure 9b along with the estimated viscosity for the asthenosphere, $\sim 10^{18}$ to 10^{19} Pa s [*Craig and McKenzie*, 1986; *Hirth and Kohlstedt*, 1996, 2004; *Karato*, 1993; *Melosh*, 1976] (Figure 9b). In Figures 9a and 9b, 30 ppm H_2O (the highest water content in olivine from the western margin of the Colorado Plateau) was assigned to the lithospheric mantle. For a constant water content, the strain rate at given depth increases with increasing stress whereas the effective viscosity decreases (Figures 9a and 9b). For comparison, we have also calculated the strain rates and equivalent effective viscosities for typical Archean cratons using the geotherm in Figure 8b and assuming 30 ppm H_2O (Figures 10a and 10b). The differences in strain rates and effective viscosities between the Colorado Plateau (Figures 9a and 9b) and typical Archean cratons (Figures 10a and 10b) largely reflect the differences in their thermal structures as shown by Figure 8b.

[40] To evaluate the effect of water on viscosity, similar calculations were done assuming constant background shear stress (0.3 MPa) but varying the water contents (Figure 9c and 9d) for the Colorado Plateau and Figures 10c and 10d for Archean cratons). A maximum value for viscosity was determined by considering a dry lithosphere (we used ~10 ppm H_2O, corresponding to ~150 H/10^6 Si atoms, to represent a dry lithosphere [*Hirth and Kohlstedt*, 2004; *Mei and Kohlstedt*, 2000]). A minimum for the viscosity was calculated at water-saturated conditions, with water solubility and thermal state taken from Figure 8b. If the average viscosity estimated for the asthenosphere (~5×10^{18} Pa s, the vertical lines in Figures 9b and 9d) were used to mark the lithosphere-asthenosphere boundary, our calculations predict that beneath the Colorado Plateau a dry lithosphere will extend to a depth of ~120 km (Figure 9d) comparing to ~250 km beneath Archean cratons (Figure 10d).

[41] The effect of adding ~45 ppm H_2O (the highest water content in olivine from the central Colorado Plateau, Figure 1) is to decrease the effective viscosity by around 1 order of magnitude at the base of the lithosphere for both the Colorado Plateau (at ~120 km depth, Figure 9d) and Archean cratons (at ~250 km depth, Figure 10d). Such decreases in viscosity translate into reductions in effective lithospheric thicknesses as illustrated along the line representing the average asthenospheric viscosity in Figures 9d and 10d. Adding 45 ppm H_2O (in olivine) results in a reduction of effective lithospheric thickness of ~ 12 km and ~30 km for the Colorado Plateau and Archean cratons, respectively. The original lithospheric thicknesses for the Colorado Plateau and Archean cratons being estimated at ~120 km and 250 km respectively, rehydration alone could have resulted in ~10% or more lithospheric thinning. In a cratonic lithosphere (~250 km thick) under water-saturated condition (without considering hydrous melting in this case), up to ~100 km of lithospheric thinning can be achieved (Figure 10d). Moreover, the extent of lithospheric thinning may be further enhanced after the weakened basal lithosphere (of viscosity $<5 \times 10^{18}$ Pa s say) is entrained by convective currents, which leads to the exposure of the asthenosphere to hydrated lithosphere at shallower depths. Repeating the above calculations using equation (5) [after *Hirth and Kohlstedt*, 2004] predicts identical lithospheric thinning effects as comparing to using equation (4) (Figure 9d).

[42] In summary, strain rates, effective viscosities and thus effective lithospheric thicknesses for the lithospheric mantle depend on a combination of temperature, shear stress and water content. Only moderate hydration (addition of ~45 ppm H_2O into olivine) is needed to weaken the lithosphere and initiate lithospheric thinning. Up to ~100 km of lithospheric thinning can be achieved underneath cratons when water-saturated conditions are assumed and hydrous melting is ignored.

6. Speculations

[43] The present lithospheric thicknesses as constrained by seismic studies are ~50 to 60 km beneath the southern Basin and Range [*West et al.*, 2004; *Zandt et al.*, 1995] and ~120 to 150 km beneath the Colorado Plateau [*West et al.*, 2004]. The lithospheric thickness beneath the Great Plains (an undeformed part of the North American Craton), however, is estimated to be ~200 km [*West et al.*, 2004]. If we assume that much of the North American craton was originally thick (say, ~200 km), extensive lithospheric thinning (>50 to 100 km) must have occurred beneath the Colorado Plateau and Basin and Range (note that the original thickness beneath the Basin and Range, while thicker than present, may not have been as thick as typical Archean cratons [*Lee et al.*, 2001a]). A number of hypotheses have been suggested to give rise to lithospheric thinning: (1) buoyancy-driven delamination [*Bird*, 1979; *Jull and Kelemen*, 2001; *Kay and Kay*, 1993; *Moore et al.*, 2005; *Poudjom Djomani et al.*, 2001; *Schott and*

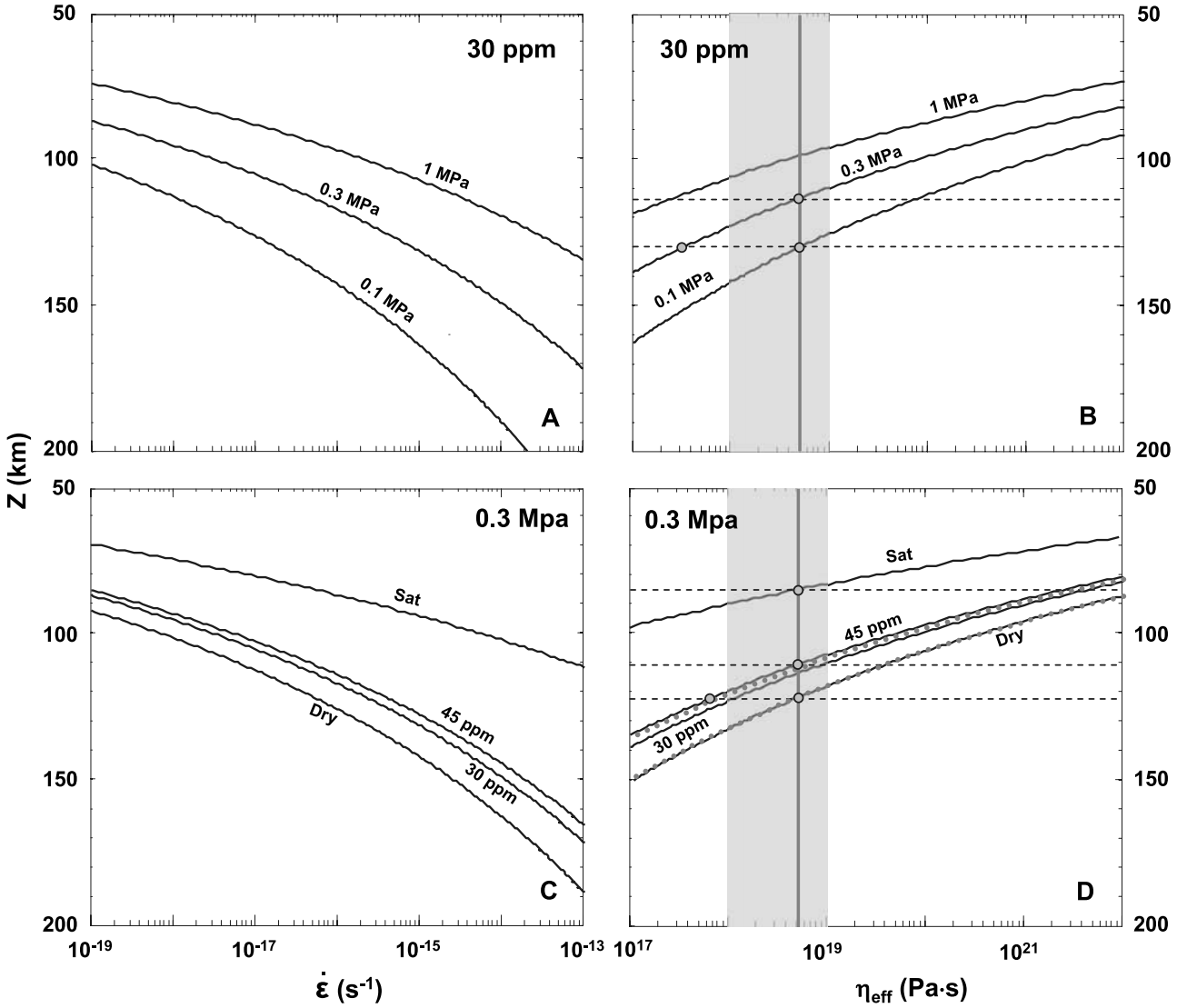

Figure 9. Calculated strain rates and effective viscosities η_{eff} of the lithospheric mantle beneath the Colorado Plateau (using equation (4)). (a) Strain rates versus depth at various shear stresses (0.1, 0.3, and 1 MPa, respectively) assuming homogeneous water content (30 ppm H_2O). (b) Effective viscosities η_{eff} versus depth corresponding to Figure 9a. (c) Strain rates versus depth at constant shear stress (0.3 MPa) assuming various water contents. Dry, effectively dry condition, approximated by assigning ~10 ppm H_2O to olivine [*Mei and Kohlstedt*, 2000]; 30 ppm and 45 ppm, the highest measured water contents in olivines from the Grand Canyon (western margin of the Colorado Plateau) and Navajo (central Colorado Plateau), respectively (Figure 1); Sat, water-saturated condition, H_2O contents are constrained by solubility curve in Figure 8b. (d) Effective viscosities η_{eff} versus depth corresponding to C. Shaded regions in Figures 9b and 9d are the estimated viscosity range for the asthenosphere [*Craig and McKenzie*, 1986; *Hirth and Kohlstedt*, 1996; *Hirth and Kohlstedt*, 2004; *Karato*, 1993; *Melosh*, 1976] with an average of 5×10^{18} Pa s (the vertical lines). For comparison, calculations using equation (5) [after *Hirth and Kohlstedt*, 2004] for dry and 45 ppm H_2O scenarios are plotted in Figure 9d as dotted gray curves.

Schmeling, 1998], (2) basal erosion due to enhanced thermal and/or mechanical disruptions [*Bird*, 1984, 1988; *Davies*, 1994; *Deng et al.*, 1998; *Griffin et al.*, 1998; *Menzies et al.*, 1993; *Xu*, 2001], and (3) lithospheric extension [*Wernicke et al.*, 1988]. In the case of the western North America, the flat subduction of the Farallon slab has been suggested to have truncated the overriding continental lithosphere [*Bird*, 1984, 1988]. The flat subduction of the Farallon slab, however, also introduced water into the North American lithospheric mantle [*Humphreys et al.*, 2003; *Lee*, 2005; *Smith et al.*, 1999; *Smith*, 2000; *Smith et al.*, 2004; *Smith and Griffin*, 2005]. Our FTIR study confirms that the lithospheric mantle beneath the Colorado Plateau appears to be wetter than typical continental lithosphere and the ambient convecting mantle (the MORB source, Figure 1). We speculate that hydration-induced lithospheric thinning might have further modified the western North American lithosphere and thus, along with slab truncation [*Bird*, 1984, 1988] accounts for

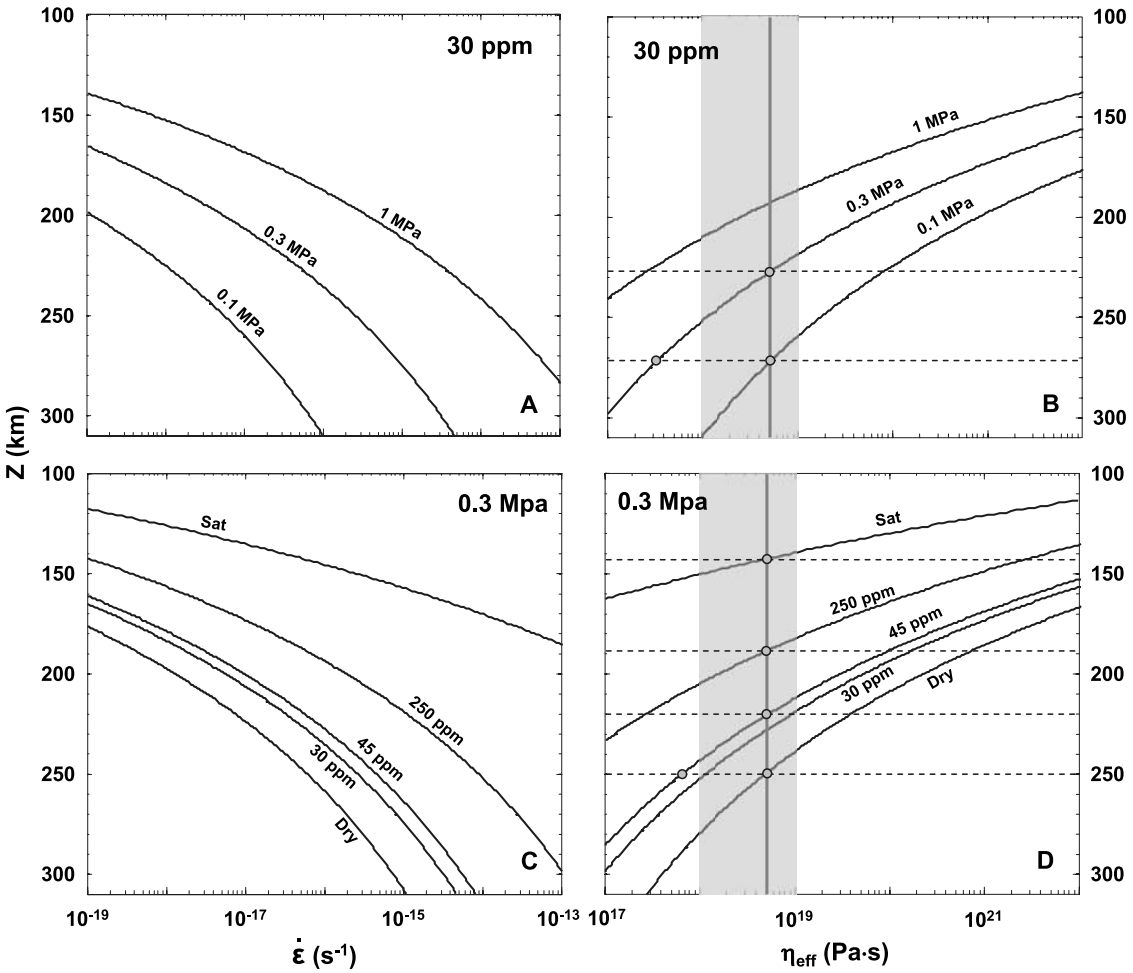

Figure 10. Calculated strain rates and effective viscosities η_{eff} of the lithospheric mantle beneath Archean cratons (using equation (4)). (a) Strain rates $\dot{\varepsilon}$ versus depth at various shear stresses (0.1, 0.3, and 1 MPa, respectively) assuming homogeneous water content (30 ppm H_2O). (b) Effective viscosities η_{eff} versus depth corresponding to Figure 10a. (c) Strain rates $\dot{\varepsilon}$ versus depth at constant shear stress (0.3 MPa) assuming various water contents. Dry, effectively dry condition, approximated by assigning ~10 ppm H_2O to olivine [*Mei and Kohlstedt*, 2000]; 30 and 45 ppm, the highest measured water contents in olivines from the Grand Canyon (western margin of the Colorado Plateau) and Navajo (central Colorado Plateau), respectively (Figure 1); 250 ppm, the maximal amount of water olivine can hold at ~150 km depth (within subridge lithospheric mantle) without triggering hydrous melting (assuming a peridotite stoichiometry: ~60% olivine, ~30% orthopyroxene, and ~10% clinopyroxene and using the results of *Aubaud et al.* [2004], partition coefficients were revised according to new calibration in *Aubaud et al.* [2007]); Sat, water-saturated condition, H_2O contents are constrained by solubility curve in Figure 8b. (d) Effective viscosities η_{eff} versus depth corresponding to Figure 10c. Shaded regions in Figures 10b and 10d are the estimated viscosity range for the asthenosphere [*Craig and McKenzie*, 1986; *Hirth and Kohlstedt*, 1996; *Hirth and Kohlstedt*, 2004; *Karato*, 1993; *Melosh*, 1976] with an average of 5×10^{18} Pa s (the vertical lines).

its present-day lithospheric structure. Because the effect of water on lithospheric thickness is magnified at greater depths and at higher water contents (Figures 9 and 10), the hydration-induced lithospheric thinning inferred here for the western North America may have played a more significant role in modifying continents with thicker lithosphere, such as cratons. If so, subduction-induced hydration could lead to the weakening, thinning and eventual dissociation and recycling of cratons on a global scale.

[44] **Acknowledgments.** This research was supported by the NSF (EAR-0635668) and the Packard Foundation. Peter Luffi, Xin Cheng, Yang He, and Tobias Höink are thanked for discussions. Critical and constructive reviews by Greg Hirth, Jacqueline Dixon, and Reid Cooper are greatly appreciated.

References

Asimow, P. D., M. M. Hirschmann, and E. M. Stolper (2001), Calculation of peridotite partial melting from thermodynamic models of minerals and melts, IV. Adiabatic decompression and the composition and mean properties of mid-ocean ridge basalts, *J. Petrol.*, *42*, 963–998, doi:10.1093/petrology/42.5.963.

Aubaud, C., E. H. Hauri, and M. M. Hirschmann (2004), Hydrogen partition coefficients between nominally anhydrous minerals and basaltic melts, *Geophys. Res. Lett.*, *31*, L20611, doi:10.1029/2004GL021341.

Aubaud, C., A. C. Withers, M. M. Hirschmann, Y. Guan, L. A. Leshin, S. Mackwell, and D. Bell (2007), Intercalibration of FTIR and SIMS for hydrogen measurements in glasses and nominally anhydrous minerals, *Am. Mineral.*, *92*, 811–828, doi:10.2138/am.2007.2248.

Bai, Q., and D. L. Kohlstedt (1992), Substantial hydrogen solubility in olivine and implications for water storage in the mantle, *Nature*, *357*, 672–674, doi:10.1038/357672a0.

Bai, Q., and D. L. Kohlstedt (1993), Effects of chemical environment on the solubility and incorporation mechanism for hydrogen in olivine, *Phys. Chem. Miner.*, *19*, 460–471, doi:10.1007/BF00203186.

Bell, D. R., and G. R. Rossman (1992), Water in Earth's mantle: The role of nominally anhydrous minerals, *Science*, *255*, 1391–1397, doi:10.1126/science.255.5050.1391.

Bell, D. R., P. D. Ihinger, and G. R. Rossman (1995), Quantitative analysis of trace OH in garnet and pyroxenes, *Am. Mineral.*, *80*, 465–474.

Bell, D. R., G. R. Rossman, J. Maldener, D. Endisch, and F. Rauch (2003), Hydroxide in olivine: A quantitative determination of the absolute amount and calibration of the IR spectrum, *J. Geophys. Res.*, *108*(B2), 2105, doi:10.1029/2001JB000679.

Bennett, V. C., and D. J. DePaolo (1987), Proterozoic crustal history of the western United States as determined by neodymium isotopic mapping, *Geol. Soc. Am. Bull.*, *99*, 674–685, doi:10.1130/0016-7606(1987)99<674:PCHOTW>2.0.CO;2.

Bird, P. (1979), Continental delamination and the Colorado Plateau, *J. Geophys. Res.*, *84*, 7561–7571.

Bird, P. (1984), Laramide crustal thickening event in the Rocky Mountains foreland and Great Plains, *Tectonics*, *3*, 741–758, doi:10.1029/TC003i007p00741.

Bird, P. (1988), Formation of the Rocky Mountains, western United States: A continuum computer model, *Science*, *239*, 1501–1507, doi:10.1126/science.239.4847.1501.

Brey, G. P., and T. Köhler (1990), Geothermobarometry in four-phase lherzolites II. New thermobarometers, and practical assessment of existing thermobarometers, *J. Petrol.*, *31*, 1353–1378.

Brey, G. P., T. Köhler, and K. G. Nickel (1990), Geothermobarometry in four-phase lherzolites I. Experimental results from 10 to 60 kb, *J. Petrol.*, *31*, 1313–1352.

Chopra, P. N., and M. S. Paterson (1984), The role of water in the deformation of dunite, *J. Geophys. Res.*, *89*, 7861–7876, doi:10.1029/JB089iB09p07861.

Craig, C. H., and D. McKenzie (1986), The existence of a thin low-viscosity layer beneath the lithosphere, Earth Planet, *Sci. Lett.*, *78*, 420–426, doi:10.1016/0012-821X(86)90008-7.

Daley, E. E., and D. J. DePaolo (1992), Isotopic evidence for lithospheric thinning during extension: Southeastern Great Basin, *Geology*, *20*, 104–108, doi:10.1130/0091-7613(1992)020<0104:IEFLTD>2.3.CO;2.

Danyushevsky, L. V., S. M. Eggins, T. J. Fallon, and D. M. Christie (2000), H_2O abundance in depleted to moderately enriched mid-ocean ridge magmas. Part I: Incompatible behaviour, implications for mantle storage, and origin of regional variations, *J. Petrol.*, *41*, 1329–1364, doi:10.1093/petrology/41.8.1329.

Davies, G. F. (1994), Thermomechanical erosion of the lithosphere by mantle plumes, *J. Geophys. Res.*, *99*, 15,709–15,722, doi:10.1029/94JB00119.

Demouchy, S., S. D. Jacobsen, F. Gaillard, and C. R. Stern (2006), Rapid magma ascent recorded by water diffusion profiles in mantle olivine, *Geology*, *34*(6), 429–432, doi:10.1130/G22386.1.

Deng, J. F., H. L. Zhao, Z. Luo, Z. Guo, and X. Mo (1998), Mantle plumes and lithosphere motion in East Asia, in *Mantle Dynamics and Plate Interactions in East Asia*, *Geodyn. Ser.*, vol. 27, edited by M. Flower et al., pp. 59–66, AGU, Washington, D. C.

Dickinson, W. R. (2004), Evolution of the North American Cordillera, *Annu. Rev. Earth Plan et. Sci.*, *32*, 13–45, doi:10.1146/annurev.earth.32.101802.120257.

Dickinson, W. R., and W. S. Snyder (1978), Plate tectonics of the Laramide orogeny, in *Laramide Folding Associated With Basement Block Faulting in the Western United States*, edited by V. Matthews, *Mem. Geol. Soc. Am.*, *151*, 355–366.

Dixon, J. E., E. Stolper, and J. R. Delaney (1988), Infrared spectroscopic measurements of CO_2 and H_2O in Juan de Fuca basaltic glasses, *Earth Planet. Sci. Lett.*, *90*, 87–104, doi:10.1016/0012-821X(88)90114-8.

Dixon, J. E., D. A. Clague, P. Wallace, and R. J. Poreda (1997), Volatiles in alkalic basalts from the North Arch Volcanic Field, Hawaii: Extensive degassing of deep submarine-erupted alkalic series lavas, *J. Petrol.*, *38*, 911–939, doi:10.1093/petrology/38.7.911.

Dixon, J. E., L. Leist, C. Langmuir, and J.-G. Schilling (2002), Recycled dehydrated lithosphere observed in plume-influenced mid-ocean-ridge basalt, *Nature*, *420*, 385–389, doi:10.1038/nature01215.

Dixon, J. E., T. H. Dixon, D. R. Bell, and R. Malservisi (2004), Lateral variation in upper mantle viscosity: Role of water, *Earth Planet. Sci. Lett.*, *222*, 451–467, doi:10.1016/j.epsl.2004.03.022.

Doin, M.-P., L. Fleitout, and U. Christensen (1997), Mantle convection and stability of depleted and undepleted continental lithosphere, *J. Geophys. Res.*, *102*, 2771–2787, doi:10.1029/96JB03271.

Ehrenberg, S. N. (1982a), Petrogenesis of garnet lherzolite and megacrystalline nodules from the Thumb, Navajo volcanic field, *J. Petrol.*, *23*, 507–547.

Ehrenberg, S. N. (1982b), Rare earth element geochemistry of garnet lherzolite and megacrystalline nodules from minette of the Colorado Plateau province, *Earth Planet. Sci. Lett.*, *57*(1), 191–210, doi:10.1016/0012-821X(82)90185-6.

Engebretson, D. C., A. Cox, and R. G. Gordon (1985), Relative motions between oceanic and continental plates in the Pacific basin, *Spec. Pap. Geol. Soc. Am.*, *206*, 59 pp..

English, J. M., S. T. Johnston, and K. Wang (2003), Thermal modelling of the Laramide orogeny: Testing the flat-slab subduction hypothesis, *Earth Planet. Sci. Lett.*, *214*, 619–632, doi:10.1016/S0012-821X(03)00399-6.

Fei, Y. (1995), Thermal expansion, in *Mineral Physics and Crystallography*, *AGU Ref. Shelf*, vol. 2, edited by T. J. Ahrens, pp. 29–44, AGU, Washington, D. C.

Grant, K. J., J. Ingrin, J. P. Lorand, and P. Dumas (2007a), Water partitioning between mantle minerals from peridotite xenoliths, *Contrib. Mineral. Petrol.*, *154*, 15–34, doi:10.1007/s00410-006-0177-1.

Grant, K. J., S. C. Kohn, and R. A. Brooker (2007b), The partitioning of water between olivine, orthopyroxene and melt synthesised in the system albite-forsterite-H_2O, *Earth Planet. Sci. Lett.*, *260*, 227–241, doi:10.1016/j.epsl.2007.05.032.

Griffin, W. L., A. Zhang, S. Y. O'Reilly, and C. G. Ryan (1998), Phanerozoic evolution of the lithosphere beneath the Sino-Korean craton, in *Mantle Dynamics and Plate Interactions in East Asia*, *Geodyn. Ser.*, vol. 27, edited by M. F. J. Flower et al., pp. 107–126, AGU, Washington, D. C.

Griffin, W. L., S. Y. O'Reilly, and C. G. Ryan (1999), The composition and origin of sub-continental lithospheric mantle, in *Mantle Petrology: Field Observations and High Pressure Experimentation: A Tribute to R. (Joe) Boyd*, edited by Y. Fei, C. M. Bertka, and B. O. Mysen, *Spec. Publ. Geochem. Soc. 6*, 13–45.

Griffin, W. L., S. Y. O'Reilly, N. Abe, S. Aulbach, R. M. Davies, N. J. Pearson, B. J. Doyle, and K. Kivi (2003), The origin and evolution of Archean lithospheric mantle, *Precambrian Res.*, *127*, 19–41, doi:10.1016/S0301-9268(03)00180-3.

Hauri, E. H. (2002), SIMS analysis of volatiles in silicate glasses; 2: Isotopes and abundances in Hawaiian melt inclusions, *Chem. Geol.*, *183*, 115–141, doi:10.1016/S0009-2541(01)00374-6.

Hauri, E. H., G. A. Gaetani, and T. H. Green (2006), Partitioning of water during melting of the Earth's upper mantle at H_2O-undersaturated conditions, *Earth Planet. Sci. Lett.*, *248*, 715–734, doi:10.1016/j.epsl.2006.06.014.

Hawkesworth, C. J., , and M. J. Norry (Eds.) (1983), *Continental Basalts and Mantle Xenoliths*, 272 pp., Shiva, Cheshire, U.K.

Hercule, S., and J. Ingrin (1999), Hydrogen in diopside: Diffusion, kinetics of extraction-incorporation, and solubility, *Am. Mineral.*, *84*, 1577–1587.

Hirschmann, M. M. (2006), Water, melting, and the deep earth H_2O cycle, *Annu. Rev. Earth Planet. Sci.*, *34*, 629–653, doi:10.1146/annurev.earth.34.031405.125211.

Hirth, G., and D. L. Kohlstedt (1996), Water in the oceanic upper mantle: Implications for rheology, melt extraction and the evolution of the lithosphere, *Earth Planet. Sci. Lett.*, *144*(1–2), 93–108, doi:10.1016/0012-821X(96)00154-9.

Hirth, G., and D. L. Kohlstedt (2004), Rheology of the upper mantle and the mantle wedge: A view from the experimentalists, in *Inside the Subduction Factory*, *Geophys. Monogr. Ser.*, vol. 138, edited by J. Eiler, pp. 83–106, AGU, Washington, D. C.

Hirth, G., R. L. Evans, and A. D. Chave (2000), Comparison of continental and oceanic mantle electrical conductivity: Is the Archean lithosphere dry?, *Geochem. Geophys. Geosyst.*, *1*(12), 1030, doi:10.1029/2000GC000048.

Humphreys, E. D., E. Hessler, K. G. Dueker, G. L. Farmer, E. A. Erslev, and T. A. Atwater (2003), How Laramide-age hydration of North American lithosphere by the Farallon slab controlled subsequent activity in the western United States, *Int. Geol. Rev.*, *45*, 575–595, doi:10.2747/0020-6814.45.7.575.

Ingrin, J., and H. Skogby (2000), Hydrogen in nominally anhydrous upper-mantle minerals: Concentration levels and implications, *Eur. J. Mineral.*, *12*, 543–570.

Ingrin, J., S. Hercule, and T. Charton (1995), Diffusion of hydrogen in diopside: Results of dehydration experiments, *J. Geophys. Res.*, *100*, 15489–15,499, doi:10.1029/95JB00754.

Jamtveit, B., R. Brooker, K. Brooks, L. M. Larsen, and T. Pedersen (2001), The water content of olivines from the North Atlantic Volcanic Province,, *Earth Planet. Sci. Lett.*, *186*, 401–415, doi:10.1016/S0012-821X(01)00256-4.

Jordan, T. H. (1975), The continental tectosphere, *Rev. Geophys.*, *13*, 1–12, doi:10.1029/RG013i003p00001.

Jordan, T. H. (1978), Composition and development of the continental tectosphere, *Nature*, *274*, 544–548, doi:10.1038/274544a0.

Jull, M., and P. Kelemen (2001), On the conditions for lower crustal convective instability, *J. Geophys. Res.*, *106*, 6423–6446, doi:10.1029/2000JB900357.

Karato, S. (1993), Rheology of the upper mantle: A synthesis, *Science*, *260*, 771–778, doi:10.1126/science.260.5109.771.

Karato, S.-I., and P. Wu (1993), Rheology of the upper mantle, *Science*, *260*, 771–778, doi:10.1126/science.260.5109.771.

Kay, R. W., and S. M. Kay (1993), Delamination and delamination magmatism, *Tectonophysics*, *219*, 177–189, doi:10.1016/0040-1951(93)90295-U.

Kelley, K. A., T. Plank, T. L. Grove, E. M. Stolper, S. Newman, and E. Hauri (2006), Mantle melting as a function of water content beneath back-arc basins, *J. Geophys. Res.*, *111*, B09208, doi:10.1029/2005JB003732.

Kinzler, R. J., and T. L. Grove (1992), Primary magmas of mid-ocean ridge basalts: 2. Applications, *J. Geophys. Res.*, *97*, 6907–6926.

Kohlstedt, D. L., and S. J. Mackwell (1998), Diffusion of hydrogen and intrinsic point defects in olivine, *Z. Phys. Chem.*, *207*, 147–162.

Kohlstedt, D. L., B. Evans, and S. J. Mackwell (1995), Strength of the lithosphere: Constraints imposed by laboratory experiments, *J. Geophys. Res.*, *100*, 17,587–17,602, doi:10.1029/95JB01460.

Kohlstedt, D. L., H. Keppler, and D. C. Rubie (1996), Solubility of water in the α, β and γ phases of $(Mg, Fe)_2SiO_4$, *Contrib. Mineral. Petrol.*, *123*, 345–357, doi:10.1007/s004100050161.

Lee, C.-T. A. (2005), Trace element evidence for hydrous metasomatism at the base of the North American Lithosphere and possible association with Laramide low-angle subduction, *J. Geol.*, *113*, 673–685, doi:10.1086/449327.

Lee, C.-T. (2006), Geochemical/petrologic constraints on the origin of cratonic mantle, in *Archean Geodynamics and Environments*, *Geophys. Monogr. Ser.*, vol. 164, edited by K. Benn et al., pp. 89-114, AGU, Washington, D. C.

Lee, C.-T., and W.-P. Chen (2007), Possible density segregation of subducted oceanic lithosphere along a weak serpentinite layer and implications for compositional stratification of the Earth's mantle, *Earth Planet. Sci. Lett.*, *255*, 357–366, doi:10.1016/j.epsl.2006.12.022.

Lee, C.-T., R. L. Rudnick, and G. H. Brimhall Jr. (2001a), Deep lithospheric dynamics beneath the Sierra Nevada during the Mesozoic and Cenozoic as inferred from xenolith petrology, *Geochem. Geophys. Geosyst.*, *2*(12), 1053, doi:10.1029/2001GC000152.

Lee, C.-T., Q. Yin, R. L. Rudnick, and S. B. Jacobsen (2001b), Preservation of ancient and fertile lithospheric mantle beneath the southwestern United States, *Nature*, *411*, 69–73, doi:10.1038/35075048.

Lee, C.-T., A. Lenardic, C. M. Cooper, F. Niu, and A. Levander (2005), The role of chemical boundary layers in regulating the thickness of continental and oceanic thermal boundary layers, *Earth Planet. Sci. Lett.*, *230*, 379–395, doi:10.1016/j.epsl.2004.11.019.

Lenardic, A., and L. N. Moresi (1999), Some thoughts on the stability of cratonic lithosphere: Effects of buoyancy and viscosity, *J. Geophys. Res.*, *104*, 12,747–12,759.

Lenardic, A., L.-N. Moresi, and H. Mühlhaus (2003), Longevity and stability of cratonic lithosphere: Insights from numerical simulations of coupled mantle convection and continental tectonics, *J. Geophys. Res.*, *108*(B6), 2303, doi:10.1029/2002JB001859.

Li, Z.-X. A., and C.-T. Lee (2006), Geochemical investigation of serpentinized oceanic lithospheric mantle in the Feather River Ophiolite, California: Implications for the recycling rate of water by subduction, *Chem. Geol.*, *235*, 161–185, doi:10.1016/j.chemgeo.2006.06.011.

Lipman, P. W. (1992), Magmatism in the Cordilleran United States; progress and problems, in *The Geology of North America*, vol. G3, *The Cordilleran Orogen, Conterminous U. S.*, edited by B. C. Burchfiel, P. W. Lipman, and M. L. Zoback, pp. 481–514, Geol. Soc. of Am., Boulder, Colo.

Mackwell, S. J., and D. L. Kohlstedt (1990), Diffusion of hydrogen in olivine: Implications for water in the mantle, *J. Geophys. Res.*, *95*, 5079–5088, doi:10.1029/JB095iB04p05079.

Mackwell, S. J., D. L. Kohlstedt, and M. S. Paterson (1985), The role of water in the deformation of olivine single crystals, *J. Geophys. Res.*, *90*, 11,319–11,333, doi:10.1029/JB090iB13p11319.

McKenzie, D., and M. J. Bickle (1988), The volume and composition of melt generated by extension of the lithosphere, *J. Petrol.*, *29*, 625–679.

Mei, S., and D. L. Kohlstedt (2000), Influence of water on plastic deformation of olivine aggregates: 2. Dislocation creep regime, *J. Geophys. Res.*, *105*, 21,471–21,481, doi:10.1029/2000JB900180.

Melosh, H. J. (1976), Nonlinear stress propagation in the Earth's upper mantle, *J. Geophys. Res.*, *81*, 5621–5632, doi:10.1029/JB081i032p05621.

Menzies, M. A., and C. J. Hawkesworth (Eds.) (1987), *Mantle Metasomatism*, 472 pp., Academic, London.

Menzies, M. A., W. Fan, and M. Zhang (1993), Palaeozoic and Cenozoic lithoprobes and the loss of >120 km of Archaean lithosphere, Sino-Korean craton, China, in *Magmatic Processes and Plate Tectonics*, edited by H. M. Prichard et al., *Geol. Soc. Spec. Publ.*, *76*, 71–81.

Michael, P. J. (1988), The concentration, behavior and storage of H_2O in the suboceanic upper mantle: Implications for mantle metasomatism, *Geochim. Cosmochim. Acta*, *52*, 555–566, doi:10.1016/0016-7037(88)90110-X.

Michael, P. (1995), Regionally distinctive sources of depleted MORB: Evidence from trace elements and H_2O, *Earth Planet. Sci. Lett.*, *131*, 301–320, doi:10.1016/0012-821X(95)00023-6.

Mierdel, K., H. Keppler, J. R. Smyth, and F. Langenhorst (2007), Water solubility in aluminous orthopyroxene and the origin of Earth's asthenosphere, *Science*, *315*, 364–368, doi:10.1126/science.1135422.

Miller, G. H., G. R. Rossman, and G. E. Harlow (1987), The natural occurrence of hydroxyle in olivine, *Phys. Chem. Miner.*, *14*, 461–472, doi:10.1007/BF00628824.

Moore, V. M., B. C. Vendeville, and D. V. Wiltschko (2005), Effects of buoyancy and mechanical layering on collisional deformation of continental lithosphere: Results from physical modeling, *Tectonophysics*, *403*, 193–222, doi:10.1016/j.tecto.2005.04.004.

Mosenfelder, J. L., T. G. Sharp, P. D. Asimow, and G. R. Rossman (2006), Hydrogen incorporation in natural mantle olivines, in *Earth's Deep Water Cycle, Geophys. Monogr. Ser.*, vol. 168, edited by S. D. Jacobsen and S. van der Lee, pp. 45–56, AGU, Washington, D. C.

Navrotsky, A. (1995), Thermodynamic properties of minerals, in *Mineral Physics and Crystallography: A Handbook of Physical Constants*, *AGU Ref. Shelf*, vol. 2, edited by T. J. Ahrens, pp. 18–28, AGU, Washington, D. C.

Nichols, A. R. L., M. R. Carroll, and A. Höskuldsson (2002), Is the Iceland hot spot also wet? Evidence from the water contents of undergassed submarine and subglacial pillow basalts, *Earth Planet. Sci. Lett.*, *202*, 77–78, doi:10.1016/S0012-821X(02)00758-6.

Nixon, P. H. (Ed.) (1987), *Mantle Xenoliths*, 844 pp., John Wiley, New York.

Paterson, M. (1982), The determination of hydroxyl by infrared absorption in quartz, silicate glasses and minerals, *Bull. Mineral.*, *105*, 20–29.

Pearson, D. G., R. W. Carlson, S. B. Shirey, F. R. Boyd, and P. H. Nixon (1995), Stabilization of Archean lithospheric mantle: A Re-Os isotope study of peridotite xenoliths from the Kaapvaal craton, *Earth Planet. Sci. Lett.*, *134*, 341–357, doi:10.1016/0012-821X(95)00125-V.

Peslier, A. H., and J. F. Luhr (2006), Hydrogen loss from olivines in mantle xenoliths from Simcoe (USA) and Mexico: Mafic alkalic magma ascent rates and water budget of the sub-continental lithosphere, *Earth Planet. Sci. Lett.*, *242*, 302–319, doi:10.1016/j.epsl.2005.12.019.

Peslier, A. H., J. F. Luhr, and J. Post (2002), Low water contents in pyroxenes from spinel-seridotites of the oxidized, sub-arc mantle wedge, *Earth Planet. Sci. Lett.*, *201*, 69–86, doi:10.1016/S0012-821X(02)00663-5.

Pitzer, K. S., and S. M. Sterner (1994), Equations of state valid continuously from zero to extreme pressures for H_2O and CO_2, *J. Chem. Phys.*, *101*(4), 3111–3116, doi:10.1063/1.467624.

Pollack, H. N. (1986), Cratonization and thermal evolution of the mantle, *Earth Planet. Sci. Lett.*, *80*, 175–182, doi:10.1016/0012-821X(86)90031-2.

Poudjom Djomani, Y. H., S. Y. O'Reilly, W. L. Griffin, and P. Morgan (2001), The density structure of subcontinental lithosphere through time, *Earth Planet. Sci. Lett.*, *184*, 605–621, doi:10.1016/S0012-821X(00)00362-9.

Presnall, D. C., G. H. Gudfinnsson, and M. J. Walter (2002), Generation of mid-ocean ridge basalts at pressures from 1 to 7 GPa, *Geochim. Cosmochim. Acta*, *66*, 2073–2090, doi:10.1016/S0016-7037(02)00890-6.

Ranero, C. R., J. Phipps Morgan, K. McIntosh, and C. Reichert (2003), Bending-related faulting and mantle serpentinization at the Middle America trench, *Nature*, *425*, 367–373, doi:10.1038/nature01961.

Riter, J. C. A., and D. Smith (1996), Xenolith constraints on the thermal history of the mantle below the Colorado Plateau, *Geology*, *24*, 267–270, doi:10.1130/0091-7613(1996)024<0267:XCOTTH>2.3.CO;2.

Roden, M. F., A. J. Irving, and V. R. Murthy (1988), Isotopic and trace element composition of the upper mantle beneath a young continental rift: Results from Kilbourne Hole, New Mexico, *Geochim. Cosmochim. Acta*, *52*, 461–473, doi:10.1016/0016-7037(88)90101-9.

Rudnick, R. L., W. F. McDonough, and R. J. O'Connell (1998), Thermal structure, thickness and composition of continental lithosphere, *Chem. Geol.*, *145*, 395–411, doi:10.1016/S0009-2541(97)00151-4.

Saal, A. E., C. H. Langmuir, and M. R. Perfit (2002), Vapour undersaturation in primitive mid-ocean-ridge basalt and the volatile content of Earth's upper mantle, *Nature*, *419*, 451–455, doi:10.1038/nature01073.

Saleeby, J. (2003), Segmentation of the Laramide Slab - evidence from the southern Sierra Nevada region, *Geol. Soc. Am. Bull.*, *115*, 655–668, doi:10.1130/0016-7606(2003)115<0655:SOTLSF>2.0.CO;2.

Sass, J. H., A. H. Lachenbruch, S. P. Galanis Jr., P. Morgan, S. S. Priest, T. H. Moses Jr., and R. J. Munroe (1994), Thermal regime of the southern Basin and Range Province: 1. Heat flow data from Arizona and the Mojave Desert of California and Nevada, *J. Geophys. Res.*, *99*, 22093–22,119, doi:10.1029/94JB01891.

Schott, B., and H. Schmeling (1998), Delamination and detachment of a lithospheric root, *Tectonophysics*, *296*, 225–247, doi:10.1016/S0040-1951(98)00154-1.

Seaman, C., S. B. Sherman, M. O. Garcia, M. B. Baker, B. Balta, and E. Stolper (2004), Volatiles in glasses from the HSDP2 drill core, *Geochem. Geophys. Geosyst.*, *5*, Q09G16, doi:10.1029/2003GC000596.

Sengor, A. M. C. (1999), Continental interiors and cratons: Any relation?, *Tectonophysics*, *305*, 1–42, doi:10.1016/S0040-1951(99)00043-8.

Shapiro, S. S., B. H. Hager, and T. H. Jordan (1999), Stability and dynamics of the continental tectosphere, *Lithos*, *48*, 135–152, doi:10.1016/S0024-4937(99)00027-4.

Simons, K., J. Dixon, J. Schilling, R. Kingsley, and R. Poreda (2002), Volatiles in basaltic glasses from the Easter-Salas y Gomez Seamount Chain and Easter Microplate: Implications for geochemical cycling of volatile elements, *Geochem. Geophys. Geosyst.*, *3*(7), 1039, doi:10.1029/2001GC000173.

Skogby, H., D. R. Bell, and G. R. Rossman (1990), Hydroxide in pyroxene: Variations in the natural environment, *Am. Mineral.*, *75*, 764–774.

Smith, D. (1995), Chlorite-rich ultramafic reaction zones in Colorado Plateau xenoliths: Recorders of sub-Moho hydration, *Contrib. Mineral. Petrol.*, *121*, 185–200, doi:10.1007/s004100050098.

Smith, D. (2000), Insights into the evolution of the uppermost continental mantle from xenolith localities on and near the Colorado Plateau and regional comparisons, *J. Geophys. Res.*, *105*, 16,769–16,781, doi:10.1029/2000JB900103.

Smith, D., and W. L. Griffin (2005), Garnetite xenoliths and mantle-water interactions below the Colorado Plateau, southwestern United States, *J. Petrol.*, *46*, 1901–1924, doi:10.1093/petrology/egi042.

Smith, D., J. C. Riter, and S. A. Mertzman (1999), Water-rock interactions, orthopyroxene growth, and Si-enrichment in the mantle: Evidence in xenoliths from the Colorado Plateau, southwestern United States, *Earth Planet. Sci. Lett.*, *165*, 45–54, doi:10.1016/S0012-821X(98)00251-9.

Smith, D., J. N. Connelly, K. Manser, D. E. Moser, T. B. Housh, F. W. McDowell, and L. E. Mack (2004), Evolution of Navajo eclogites and hydration of the mantle wedge below the Colorado Plateau, southwestern United States, *Geochem. Geophys. Geosyst.*, *5*, Q04005, doi:10.1029/2003GC000675.

Stalder, R., and H. Skogby (2003), Hydrogen diffusion in natural and synthetic orthopyroxene, *Phys. Chem. Miner.*, *30*, 12–19, doi:10.1007/s00269-002-0285-z.

Sterner, S. M., and K. S. Pitzer (1994), An equation of state for carbon dioxide valid from zero to extreme pressures, *Contrib. Mineral. Petrol.*, *117*, 362–374, doi:10.1007/BF00307271.

Taylor, J. R. (1997) *An Introduction to Error Analysis: The Study of Uncertainties in Physical Measurements*, 2nd ed., Univ. Sci. Books, Sausalito, Calif

Wallace, P. J., F. A. Frey, D. Weis, and M. F. Coffin (2002), Origin and evolution of the Kerguelen Plateau, Broken Ridge and Kerguelen Archipelago: Editorial, *J. Petrol.*, *43*, 1105–1108, doi:10.1093/petrology/43.7.1105.

Wang, K., T. Plank, J. D. Walker, and E. I. Smith (2002), A mantle melting profile across the Basin and Range, SW USA, *J. Geophys. Res.*, *107*(B1), 2017, doi:10.1029/2001JB000209.

Wells, P. R. A. (1977), Pyroxene thermometry in simple and complex systems, *Contrib. Mineral. Petrol.*, *62*, 129–139, doi:10.1007/BF00372872.

Wernicke, B. (1992), Cenozoic extensional tectonics of the U. S. Cordillera, in *The Geology of North America*, vol. G3, *The Cordilleran Orogen, Conterminous U. S.*, edited by B. C. Burchfiel, P. W. Lipman, and M. L. Zoback, pp. 553–581, Geol. Soc. of Am., Boulder, Colo.

Wernicke, B., G. J. Axen, and J. K. Snow (1988), Basin and Range extensional tectonics at the latitude of Las Vegas, Nevada, *Geol. Soc. Am. Bull.*, *100*, 1738–1757, doi:10.1130/0016-7606(1988)100<1738:BARETA>2.3.CO;2.

West, M., J. Ni, W. S. Baldridge, D. Wilson, R. Aster, W. Gao, and S. Grand (2004), Crust and upper mantle shear wave structure of the southwest United States: Implications for rifting and support for high elevation, *J. Geophys. Res.*, *109*, B03309, doi:10.1029/2003JB002575.

Wilson, D., R. Aster, M. West, J. Ni, S. Grand, W. Gao, W. S. Baldridge, S. Semken, and P. Patel (2005), Lithospheric structure of the Rio Grande rift, *Nature*, *433*, 851–855, doi:10.1038/nature03297.

Woods, S. C., S. Mackwell, and D. Dyar (2000), Hydrogen in diopside: Diffusion profiles, *Am. Mineral.*, *85*, 480–487.

Xu, Y.-G. (2001), Thermo-tectonic destruction of the Archean lithospheric keel beneath the Sino-Korean craton in China: Evidence, timing and mechanism, *Phys. Chem. Earth*, *26*(9–10), 747–757, doi:10.1016/S1464-1895(01)00124-7.

Zandt, G., S. C. Myers, and T. C. Wallace (1995), Crust and mantle structure across the Basin and Range–Colorado Plateau boundary at 37°N latitude and implications for Cenozoic extensional mechanism, *J. Geophys. Res.*, *100*, 10529–10,548, doi:10.1029/94JB03063.

Zhao, Y.-H., S. B. Ginsberg, and D. L. Kohlstedt (2004), Solubility of hydrogen in olivine: Dependence on temperature and iron content, *Contrib. Mineral. Petrol.*, *147*, 155–161, doi:10.1007/s00410-003-0524-4.

C.-T. A. Lee, A. Lenardic, and Z.-X. A. Li, Department of Earth Sciences, Rice University, 6100 Main Street, Houston, TX 77005, USA. (zxli@rice.edu)

S. J. Mackwell, Lunar and Planetary Institute, 3600 Bay Area Blvd. Houston, TX 77058, USA.

A. H. Peslier, Jacobs Technology, ESCG, Mail Code JE23, 2224 Bay Area Boulevard, Houston, TX 77058, USA.